Compressed sensing in fluorescence microscopy

Gianmaria Calisesi [a], Alberto Ghezzi [a, b], Daniele Ancora [a, *], Cosimo D'Andrea [a], Gianluca Valentini [a, b], Andrea Farina [b], Andrea Bassi [a, b]

[a] Dipartimento di Fisica, Politecnico di Milano, Piazza Leonardo da Vinci 32, 20133, Milano, Italy
[b] Istituto di Fotonica e Nanotecnologie, Consiglio Nazionale delle ricerche, Piazza Leonardo da Vinci 32, 20133, Milano, Italy

ARTICLE INFO

ABSTRACT

Compressed sensing (CS) is a signal processing approach that solves ill-posed inverse problems, from under-sampled data with respect to the Nyquist criterium. CS exploits sparsity constraints based on the knowledge of prior information, relative to the structure of the object in the spatial or other domains. It is commonly used in image and video compression as well as in scientific and medical applications, including computed tomography and magnetic resonance imaging. In the field of fluorescence microscopy, it has been demonstrated to be valuable for fast and high-resolution imaging, from single-molecule localization, super-resolution to light-sheet microscopy. Furthermore, CS has found remarkable applications in the field of mesoscopic imaging, facilitating the study of small animals' organs and entire organisms. This review article illustrates the working principles of CS, its implementations in optical imaging and discusses several relevant uses of CS in the field of fluorescence imaging from super-resolution microscopy to mesoscopy.

© 2021 The Authors. Published by Elsevier Ltd. This is an open access article under the CC BY-NC-ND license (http://creativecommons.org/licenses/by-nc-nd/4.0/).

1. Principles of compressed sensing

1.1. Introduction

Compression is extensively used in the fields of signal and image processing. When an image is acquired with a digital camera, the raw data can be several megabytes large, reflecting the millions of pixels that build the sensor. In many cases, said image can be compressed, reducing its size down to kilobytes, apparently without losing relevant information. For example, when compressing an image in JPEG or JPEG2000 format, that image is transformed by Discrete Cosine Transform (DCT) or in a wavelet basis, that can provide an accurate representation using only thousands of (non-zero) coefficients. However, the image is acquired using millions of pixels and then transformed in the new basis, introducing a storage and processing overhead.

Compressed Sensing (CS) extends the concept of compression to signal and image acquisition. It aims at acquiring only relevant information with a limited number of measurements. CS can lead to a significant reduction in the data to be captured and stored, making it a valid option in many scientific and industrial fields,

including x-ray computed tomography (Chen et al., 2008), magnetic resonance imaging (Lustig et al., 2008), (Feng et al., 2017), THz spectroscopy (Watts et al., 2014), (Chan et al., 2008), electron microscopy (Li et al., 2018), (Stevens et al., 2014), radar imaging (Baraniuk and Steeghs, 2007) and astronomy (Starck and Bobin, 2010).

In fluorescence microscopy, fewer measurements imply a lower amount of light shining the sample, thus reducing fluorophores photobleaching and tissue damages caused by overexposing (Waldchen et al., 2015). These aspects are relevant dealing with biological samples. Moreover, CS can be exploited to increase temporal resolution enabling faster acquisition at a given signal to noise ratio (SNR), making it a good choice for 4D (spatial and temporal) biological imaging. In addition, CS can be useful for multidimensional fluorescence imaging, allowing hyperspectral and lifetime imaging.

In this review article, we initially discuss the solution of linear problems, introducing the regularization that is at the basis of CS reconstructions. We then discuss its implementation in the field of optics, with particular attention to the description of the concept of *Single Pixel Camera (SPC)* and we review the applications of CS in

fluorescence imaging. Focusing on biological imaging, we discuss the use of CS at different spatial scales, from super-resolution microscopy to mesoscopy, the field of imaging that aims at studying millimetre to centimetre-scaled biological samples.

1.2. Linear sampling and ill-posed problems

Let us consider a quantity $\boldsymbol{x}$, to be sampled via the measurement matrix Φ. In the following, we can think about $\boldsymbol{x}$ as an image (or as a volumetric image) but, for the moment, it can be considered as a generic vector composed by N parameters x_n. Within Φ, each vector row $\boldsymbol{\varphi}_m$ addresses a measurement in a given basis, and it is defined by the elements φ_{nm} that sample the features located at the n-th position within $\boldsymbol{x}$. In this framework, each measurement y_m is determined by the scalar product between the measurement vector and the unknown object, as:

$$y_m = \boldsymbol{\varphi}_m \cdot \boldsymbol{x} = \sum_{n=1}^{N} \varphi_{nm} x_n \quad for \ m = 1, ..., M. \qquad 1.1$$

By measuring the sample M times, we form the vector of the measurements $\boldsymbol{y}$. In a compact notation, we can write it as a linear matrix multiplication $\boldsymbol{y} = \Phi \cdot \boldsymbol{x}$, underlying a system of linear equations that needs to be inverted to find $\boldsymbol{x}$. If the measurement basis Φ is constituted by linearly independent vectors and the number of measurements equals the number of parameters $M = N$, the system is said to be fully determined and admits a unique solution. In an experimental scenario, the presence of the noise, inaccuracies, and fluctuations of the measuring system may turn the problem to be ill-posed. The solution of the inverse problem aims to find $\boldsymbol{x}$ given $\boldsymbol{y}$ and Φ, even in the presence of noise ε, that perturbs the equation in $\boldsymbol{y} = \Phi \cdot \boldsymbol{x} + \varepsilon$. For small ε, we may assume that the measurement and the model are not too far from each other, so that $\|\boldsymbol{y} - \Phi \cdot \boldsymbol{x}\| \sim 0$. This motivates the search for a solution that minimizes the squared distance, commonly referred to as the *linear least-square problem* (for further details, a modern reference is (Ruppert, 2004)). In practical terms, we search for the parameters $\boldsymbol{x}$ that minimize the loss function:

$$\operatorname*{argmin}_{\boldsymbol{x}} \left(\sum_{m=1}^{M} |y_m - (\Phi \cdot \boldsymbol{x})_m|^2 \right) \quad \text{or equivalently}$$
$$\operatorname*{argmin}_{\boldsymbol{x}} \left(\|\boldsymbol{y} - \Phi \cdot \boldsymbol{x}\|_{l_2}^2 \right) \qquad 1.2$$

Here, a generic l_p-norm refers to the quantity $(\sum |x_n|^p)^{1/p}$ that corresponds to the Euclidean distance for $p = 2$. Compressed sensing aims at reducing the number of measurements to reconstruct the sample with $M < N$ acquisitions, in a so called under-determined measurement scheme. However, this scheme implies that the inverse problem is ill-posed (Fig. 1). The next paragraph describes how to tackle reconstructions in these conditions, introducing the concept of regularization.

1.3. Regularization of inverse problems

When an inverse problem is ill-posed, we have no guarantee neither about the existence of a solution nor about its uniqueness. A common practice to deal with ill-posedness consists in adding a priori information to the problem, forcing the solution to meet certain properties. By doing so, we restrict the optimization process towards a more stable and unique solution. This procedure is called *regularization* and it constitutes a pillar for any reconstruction in the field of CS. There are several ways to regularize the problem, but in general we can approach the problem by adding a penalty term
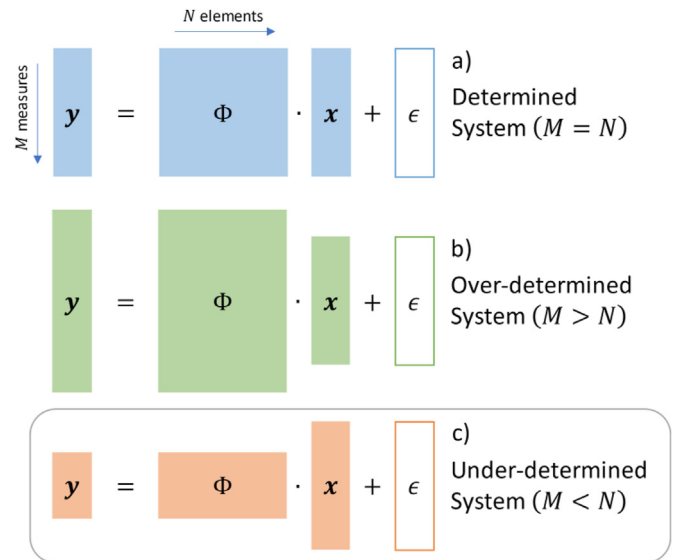

Fig. 1. Scheme for: a) determined, b) over-determined, and c) under determined problems. The CS framework is highlighted within the rectangular box and it is an ill-posed problem. CS deals with reconstructing more parameters based on just a few measurements.

to the loss function:

$$\operatorname*{argmin}_{\boldsymbol{x}} \left(\|\boldsymbol{y} - \Phi \cdot \boldsymbol{x}\|_{l_2}^2 + \tau \mathscr{R}(\boldsymbol{x}) \right), \qquad 1.3$$

Here, $\mathscr{R}(\boldsymbol{x})$ is a generic regularization rule acting on the unknown vector $\boldsymbol{x}$, and τ is a parameter to weight its contribution. When ε follows Gaussian statistics, for example, a natural choice is to look for the solution $\boldsymbol{x}$ that has the smallest Euclidean l_2-norm, defined as $\mathscr{R}(\boldsymbol{x}) = \|\boldsymbol{x}\|_{l_2}$. For CS applications, instead, the standard choice is given by the sum of all the absolute values, $\mathscr{R}(\boldsymbol{x}) = \sum_n \|x_n\| = \|\boldsymbol{x}\|_{l_1}$. The l_1-regularized problem is written as:

$$\operatorname*{argmin}_{\boldsymbol{x}} \left(\|\boldsymbol{y} - \Phi \cdot \boldsymbol{x}\|_{l_2}^2 + \tau \|\boldsymbol{x}\|_{l_1} \right) \qquad 1.4$$

The difference between the l_2 and l_1-norms may sound trivial, but it forces the solution to a completely different behaviour. From the mathematical point of view, the problem remains convex, guaranteeing that every local minimum is also a global minimum, but it does not have a closed-form solution: it is the smallest-order regularization that ensures the convexity of the linear problem (Hastie et al., 2015). Due to the lack of a direct solution, we need to approach an optimization procedure to solve it, such as gradient-descent (Ruder, 2016) or conjugate-gradient (Hager and Zhang, 2006) methods. The discussion on the best optimization strategy lies beyond the scope of the present review. Instead, we focus on its property to perform *feature selection*. Intuitively, the solution of the l_1-regularized problem returns a vector $\boldsymbol{x}$ with the smallest sum of its absolute parameters x_n. This forces the solution to reconstruct only few values, while setting all the others to zero. Hence, the procedure selects the N_s most significant parameters of the solutions, dropping all the remaining $N - N_s$ terms. Because of this peculiarity, the l_1-norm is also known as lasso-regularization (standing for "least absolute shrinkage and selection operator") or basis pursuit (Chen et al., 2001): its usage led to the exploitation of signal compression strategies. For an intuitive visual description of its action, we refer to (Romberg, 2008). It is worth mentioning that the ideal regularizer that solely accomplishes feature-selection

would be $\mathscr{R}(\boldsymbol{x}) \equiv \|\boldsymbol{x}\|_{l_0}$, which simply counts the parameters x_n different from zero. This restricts the solution of the least-square problem to the one that has the minimum number of non-null parameters. Unfortunately, this problem is not convex and the regularization with l_0 is not even a norm. Bayesian approaches have tried to deal with this by implementing a decimation procedure in the attempt to pick the minimum statistically relevant number of coefficients (Ancora and Leuzzi, 2019). However, in many practical aspects, the l_1 solution can be considered equivalent to the one that one would obtain with l_0 (Donoho and Tanner, 2009). In CS we always prefer the former, as it provides a more tractable formalism.

1.4. Sparsity, compressibility, and incoherence

The most interesting feature of the l_1-regularization concerns its ability in promoting sparsity in the solution of under-sampled systems. Rigorously, a signal is sparse when its representation in a certain basis has few non-null parameters. Operatively, the idea behind data compression is to approximate the signal without losing much of the information content. By relaxing this restriction, we extend the concept of data sparsity also to signals that exhibit just a few important parameters against others that are small but not null.

In this context, a signal is considered *compressible* (into a sparse representation) if only a few parameters are important for its description, whereas the others can be dropped without losing accuracy. In practice, if we represent $\boldsymbol{x}$ in an appropriate basis Ψ as $\boldsymbol{x} = \Psi \cdot \boldsymbol{w}$, the curve obtained by sorting the coefficient of $\boldsymbol{w}$ decays rapidly (Candes and Wakin, 2008). Two examples are provided in Fig. 2. A cleaver choice of Ψ determines how sparse the signal $\boldsymbol{w}$ is in that given basis. A consolidated approach is to expand the signal in a wavelet representation. Wavelets are functions designed to represents abrupt changes in signals (or images) that are limited in size or duration. There are several families of wavelets, but all of them begins at zero, exhibits localized oscillations, have null mean and form an orthogonal set of transformation. Thanks to these features, wavelets play a crucial role in the field of image compression, having allowed the development of the standard JPEG-2000 compression algorithm (Skodras et al., 2001). The latter is a *lossy* compression, in which a portion of information is lost due to truncation of less important wavelet coefficients. To avoid confusion, let us explicitly separate the problem into two opposite families. In case we have complete knowledge of a signal and we want to *encode* it into a compressed representation $\boldsymbol{w}$, we are talking about *signal compression*. On the other hand, if we *decode* an unknown object $\boldsymbol{x}$ from an underdetermined set of measurements, we are talking about *compressed sensing*: that is, we restore a signal from less measurements than Nyquist-Shannon sampling theorem requires.

In some cases, images may be sparse in the *xy*-coordinates and their representation into another basis Ψ is not necessary. For example, a set of individual and separated emitters acquired by a camera is already sparse in the spatial basis (like the fluorescent beads in Fig. 2a). In this case, the best representation is the identity $\Psi = I$, since a transformation may produce more coefficients than those in the direct space (Fig. 2c). Expanding a generic image, instead, into an appropriate basis (here, the wavelet basis) switches the problem of recovery in a sparser domain (Fig. 2b—d).

CS aims at sampling the object of interest $\boldsymbol{x}$ or its sparse representation $\boldsymbol{w}$ to extrapolate a reconstruction from limited acquisitions. Rather than sampling using a well-structured orthonormal Φ, it is convenient to use an *incoherent* measuring system (Candes and Wakin, 2008). Incoherent sampling relies on the fact that each measurement vector in Φ should be completely uncorrelated with respect to all the vectors in Ψ (Donoho and Huo, 2001), where the representation is assumed to be sparse. For example, the best way to sense the object of Fig. 2b would be to use functions that are maximally incoherent with respect to wavelets. These apparently random functions form the so-called noiselet transform, which is dual to wavelets, as the canonical basis is dual to the Fourier representation (Coifman et al., 2001). Intuitively, we can think about incoherent sampling as a strategy to uniformly sample the whole space. In this review we do not present the theoretical foundation of the concept behind the incoherent sampling (the advantages of which can be statistically proven (Candès et al., 2006)). The interested reader can refer to further articles that extensively analyze it on a more theoretical basis (Candès and Romberg, 2007).

1.5. Solution of inverse problems with compressed sensing

CS has been developed to investigate the solution of sparse and under-sampled linear problems. One of its most valuable result is that, from M measurements of a generic vector of length N, we can reconstruct the most important $M/\log N$ coefficients in the wavelet expansion (Candes and Tao, 2006). To obtain faithful reconstructions, CS relies on an incoherent measuring system. Here, the usage of M elements of an orthonormal basis of length N is unfeasible, because the measurement basis would be necessarily incomplete. Sparsity and incoherent sampling play a crucial role allowing the recovery of a compressed representation of the signal. To aid the search towards a sparse representation, CS makes use of the l_1-norm regularization that performs feature selection, favouring only few important features and setting all the rest to zero. In this context, sparsity, incoherence and appropriate regularization provide a framework useful to beat the Nyquist-Shannon sampling theorem (Donoho, 2006). These, seemingly simple assumptions, paved the road to several remarkable applications, particularly in the field of image reconstruction.

1.6. Limitations of compressed sensing

The advantages of CS discussed so far are given at the cost of the computational time for solving the optimization problem of Eq. (1.3). In fact, the prior typically used and discussed in Paragraph 1.3 does not allow a matrix solution and iterative methods must be implemented, thus increasing the reconstruction time. Moreover, in CS one must guess the sparsifying basis Ψ depending on the characteristics of the expected image and tune the hyperparameter
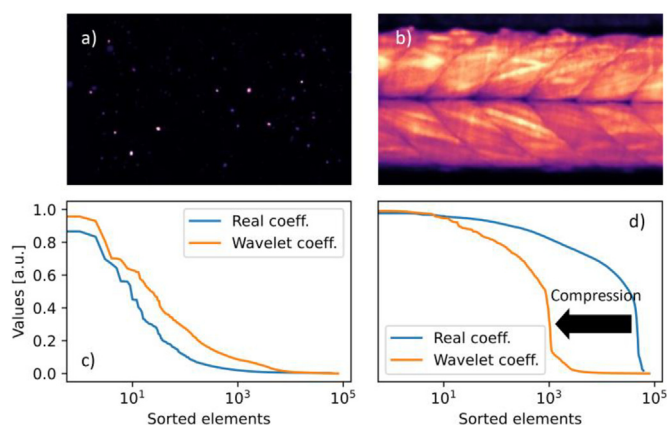

Fig. 2. a) Image of a spatially sparse object, (fluorescent beads) and c) corresponding coefficients in the direct and wavelet space. b) Image of an object (fluorescent zebrafish muscle) sparse in the wavelet space but not in the real space and d) corresponding coefficients. Few wavelet coefficients are sufficient to accurately represent the original object in panel b), but many more coefficients are required to represent the same image in the real space.

τ depending on the measurement noise and compression. All these considerations set a limit to the applicability of CS in real-time imaging because a considerable work must be done in the post-processing and image reconstruction stages. Nevertheless, in many applications, a real-time reconstruction is not needed, and CS can help to reduce the acquisition time with advantages in terms of limited sample illumination and time resolution.

To summarize, problems in CS hardly generalize, and each solution requires specific care to obtain faithful reconstructions, in particular for highly compressed measurements.

2. Implementation of compressed sensing in optical imaging

2.1. Compressed sensing in imaging

Compressed Sensing finds applications in many fields such as information theory, signal processing, computational statistics and, among others, imaging. Let us consider the case in which the signal to be sampled is two or three dimensional and can thus be represented as a 2D or 3D matrix. According to the notation introduced in Paragraph 1.2, when considering imaging applications, N is the number of points used to discretize the object plane, while M represents the number of measurements. Considering a well posed imaging problem, $M = N$ is the number of pixels at the detector. In the ideal case, the corresponding sensing matrix Φ will reproduce the object vector $\boldsymbol{x}$ at the image plane, therefore Φ is the identity matrix I with rank N. In this simple case, each point at the object plane has a unique correspondence at the image plane. Furthermore, optical systems have a characteristic Point Spread Function (PSF) and are described by a sensing matrix Φ with time invariant entries. The intensity at the detector is the convolution of the intensity at the object plane with said PSF. In this context, l_1 minimization has been successfully used for deconvolution of the blurred image (Chen et al., 2016). Notable examples are presented in references (Krishnan et al., 2011) and (Kuo et al., 2020).

Compressed sensing is used when an a-priori information about the sample is available, making it possible to reconstruct the n pixels from $m < n$ measurements. This includes cases where the sample is spatially sparse, such as in the case of single molecule, nanomaterials imaging (Zhu et al., 2012), (Xu et al., 2018) or isolated emitters (Bishara et al., 2010), (Yanny et al., 2020); spatially and temporally sparse, such as in the case of neural signals (Pégard et al., 2016) or spectrally sparse, such as in fluorescence or Raman imaging spectroscopy (Wang et al., 2017; Wadduwage et al., 2017; Wilcox et al., 2013). To refer to the number of used measurements with respect to the pixels, it is useful to define a compression ratio $CR = 1 - M/N$, expressed in percentual units.

A common way to exploit the sparsity of the problem is to use masks or spatial light modulators to structure the illumination or the detected light. Neifeld and Ke (2007) provide an overview of different optical architectures compatible with compressive imaging, comparing them in terms of bandwidth and photons budget. Among these different architectures, one popular optical scheme is the Single Pixel Camera (Duarte et al., 2008), which will be described in the next paragraphs. Since Compressed Sensing in imaging has been successfully and extensively exploited together with a single bucket detector, the presented review paper will be focused on SPC compressed protocols. Nonetheless, in the next sections they will also be introduced compressed imaging techniques where 2-dimensional detectors are used.

2.2. The single pixel camera

Imaging in the visible and near infrared (NIR) spectral range is commonly performed using CCD or CMOS cameras. These detectors

come with different sizes and features and most of them have millions of pixels, making them a feasible solution for imaging. Given their spectral properties, imaging outside of said regions requires different sensors. In many cases such sensors are not available as array or they are orders of magnitude more expensive than those used for the visible-NIR range. An approach to deal with the higher cost per pixel is to drastically lower the number of pixels needed. In this context, a possible solution is the so-called Single Pixel Camera (SPC) (Duarte et al., 2008), (Sun and Zhang, 2019). Besides being a cheap alternative, SPC is a good candidate for imaging in many different conditions, such as fluorescence, multi-spectral/hyperspectral (Studer et al., 2012), terahertz (Watts et al., 2014), polarimetric (Soldevila et al., 2013), and ultrafast (Guo et al., 2015).

In single pixel imaging, rather than directly measuring the light coming from the sample, what is acquired is the inner product between the sample spatial distribution and a family of test functions. The light reflected or emitted by the object is spatially modulated by a pattern and measured by a single pixel detector which integrates the collected light (Fig. 3a). The light is then sequentially acquired using a set of M patterns. Given a N-discretized representation of a continuous sample $\boldsymbol{x}$ and a two-dimensional family of test functions Φ, this is formally equivalent to computing the vector of projections $\boldsymbol{y} = \Phi \cdot \boldsymbol{x}$. This technique can be implemented thanks to the use of Spatial Light Modulators (SLM), which, by shaping the light (projected or collected), can generate the test function φ_m. As an alternative, arrays of Light Emitting Diodes (LED) (Salvador-Balaguer et al., 2018) can be used to modulate the illumination light and generate the required patterns.

A Spatial Light Modulator is an object that can shape the intensity (and eventually the phase) of a light beam. The light modulation can be performed in a variety of ways, according to the technology of the device. Spatial modulators have played a central
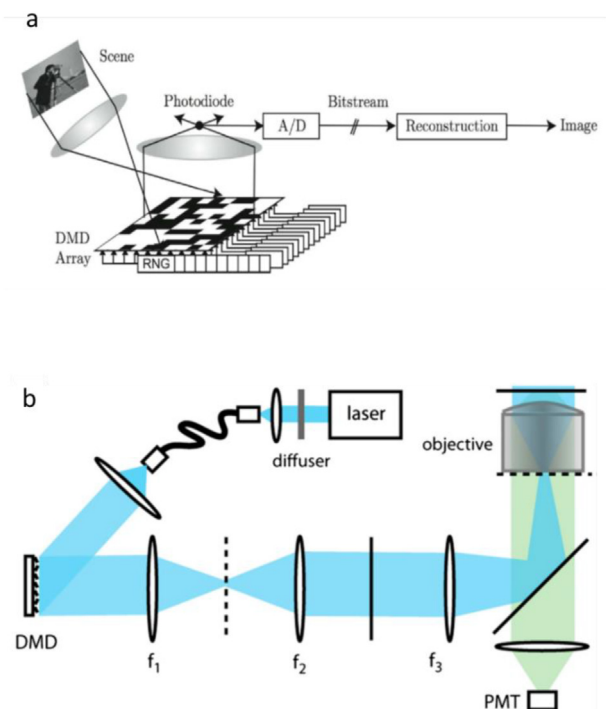

Fig. 3. Compressive imaging with a single pixel camera, © 2007 IEEE. Reprinted, with permission, from (Baraniuk, 2007) (a). Single pixel camera applied to fluorescence microscopy (b), reprinted from (Studer et al., 2012) with permission.
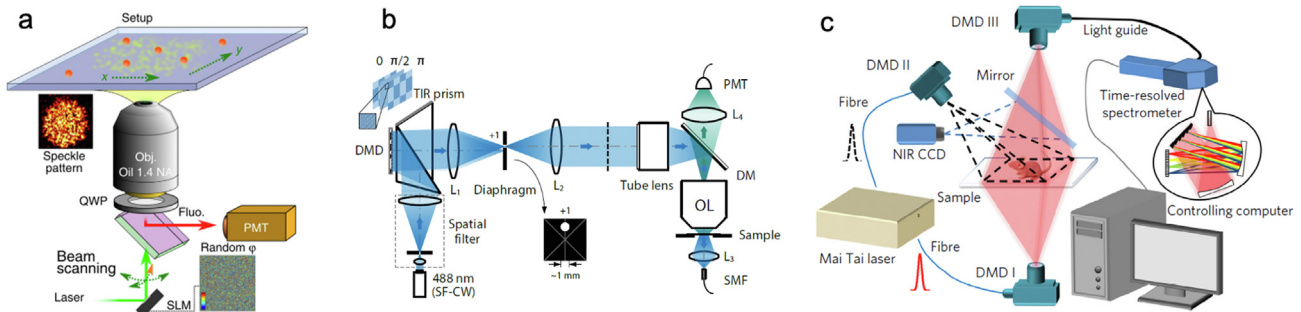
Fig. 4. CS at different spatial scales. A spatial light modulator is used to create a speckle pattern for super-resolution microscopy, reprinted from (Pascucci et al., 2019) under a Creative Commons Attribution 4.0 International License (http://creativecommons.org/licenses/by/4.0/) (a). A digital micromirror device is used for single pixel phase and fluorescence microscopy, reprinted with permission from (Liu et al., 2018) © The Optical Society (b). Multiples DMDs are used for CS mesoscopic imaging coupled with spectral and time-resolved detection, reprinted by permission from Springer Nature Customer Service Centre GmbH: Springer Nature Photonics (Pian et al., 2017) © 2017 (c).

role in the implementation of CS from super-resolution to mesoscopic imaging (Fig. 4). One of the most widespread elements for light shaping is the so called Digital Micromirror Device (DMD) (Dudley et al., 2003), a reflective spatial light modulator made by a matrix of micromirrors, usually with about a million entries, which are free to swing between two angles. The DMD can be programmed to selectively tilt the microscopic mirrors according to a desired pattern. Due to their working principle, DMDs are widely used as binary masks, with the two limit positions being interpreted as logic "0" or "1" state. Nonetheless, non-binary amplitudes can be obtained by modulating the duty cycle of the "on" logic state.

Light modulators can be alternatively placed either in the illumination or in the detection path of the imaging setup. In the first case (Fig. 3b), the DMD projects a time sequence of patterns on the sample, which is selectively illuminated, whereas in the second case, the DMD is placed in an image plane and reshapes the light coming from the sample, which is illuminated by a uniform light. However, DMDs are not the only option for spatial light modulators, as liquid crystal devices (LCD) can be also employed in single pixel camera schemes. The main feature of LCDs is the possibility to control both the amplitude and the phase of light. Hence, LCDs are mainly used in computational ghost imaging and lens-less compressive imaging systems. Nonetheless, DMDs have a higher modulation rate, lower cost and complexity. For these reasons, their use is widespread in CS imaging systems (Edgar et al., 2019).

In a Compressed Sensing acquisition scheme, the single pixel detector sequentially acquires M frames, with $M < N$, where N is the number of modulating pixels. To correctly recover the image spatial distribution, the matrix Φ must be designed so that its rows are incoherent with $\boldsymbol{x}$. Once the compressed measurement vector is obtained, an optimization algorithm is used to recover $\boldsymbol{x}$ (as formalized in Section 1). It is worth mentioning that, due to the optimization procedure, despite the compression yielded by the method, the time taken for this inversion might largely exceed the time needed to acquire $M < N$ frames. In literature, a big variety of optimization algorithm has been proposed, as l_1- norm minimization (Van Ewout Berg and Friedlander, 2008), total variation or gradient (Van Ewout Berg and Friedlander, 2008), (Figueiredo et al., 2007).

Even if random patterns perform well with most real images, compressibility can be increased with a different measurement approach, i.e., using a sampling matrix whose test functions belong to a specific basis, namely Hadamard, Wavelet and Fourier. On top of that, the subset of patterns which better captures the sample spatial features can be chosen via an a priori or a dynamic approach. Experiments have been reported in which a sub dimensioned measurement matrix was designed by assuming that adjacent frames are more likely to carry out similar spatial information (Radwell et al., 2014). In Time of Flight 3D imaging, the subset of patterns was devised with the support of a 2D range information from a coupled CCD device (Edgar et al., 2016 In other cases, this result was obtained by exploiting low resolution measurements to predict the field of view when higher resolution sampling is needed (Rousset et al., 2017), (Soldevila et al., 2015).

2.3. Selection of the patterns

As specified in the previous section, encoding spatial information on a single pixel detector is made possible by the introduction of pixelated masks, which are available to work both in reflection and transmission. The use of transmissive light modulators has been limited by the low light efficiency, nonetheless DMDs have been widely used as reflective, programmable masks with the possibility of singularly address any modulation pixel.

A possible choice of sensing matrices could be that of random measurement matrices, which are known to be incoherent with any other fixed representation basis. For their characteristics, random patterns have been used to simulate speckle patterns, as those given by diffusion in turbid media (Sun et al., 2012), even though their correlation with random waveforms (e.g., white noise) implies that a bigger number of masked measurements is needed to increase the signal to noise ratio SNR (Sun et al., 2013). As for other acquisition basis, differential measurements would also lead to a most efficient acquisition strategy, at cost of doubling the detection subsystems after the SLM.

Along with random matrices, a possible alternative is Hadamard functions. As suggested by Duarte et al. (2008), Hadamard matrices are good candidates when modulating light with DMDs. These matrices can be recursively defined by:

$$H_k = \frac{1}{\sqrt{2}} \begin{bmatrix} H_{k-1} & H_{k-1} \\ H_{k-1} & -H_{k-1} \end{bmatrix}, \qquad\qquad 2.1$$

where k is the order of the Hadamard transform and $H_0 = 1$. To define the measurement matrix, we iterate the recursion up to $k = M$. They consist of two-valued basis functions, namely $+1$ and -1, which match the modulator behaviour. Hadamard patterns show both positive and negative values, while the DMDs hardware cannot display a negative light intensity value. To encode such negative entries, it is either possible to take a differential measurement or simply to take one single positive acquisition. In the first case the Hadamard pattern is formed by subtracting two sequentially acquired complementary patterns (Harwit et al., 1979), while in the second case the acquired frames must be rescaled and

offset by the constant contribution given by a continuous illumination (Huynh et al., 2016). However, differential Hadamard measurements can be also achieved simultaneously by splitting the detection path (Soldevila et al., 2016).

Even though Hadamard patterns might not be the best choice due to their non-sparse matrix shape and the resulting storage needed (Sun et al., 2017), given any k-dimensional Hadamard matrix it holds that $H_k H_k^T = kI_k$, meaning that well posed problems with such matrix do not need matrix inversion. On top of that, the heavy computation needed for dense matrix-vector product can be bypassed by the fast Walsh-Hadamard transform, which requires a computational complexity of $M log(M)$, instead of $O(M^2)$ (Geadah and Corinthios, 1977).

Another option for the measurement matrix can be that of Fourier patterns. These patterns have been widely deployed both in super resolution imaging (Gustafsson, 2000), (Dan et al., 2013) and single pixel imaging (Zhang et al., 2015). Differently from Hadamard matrices, Fourier transform basis also have nonbinary entries which can be DMD encoded by dithering the micromirrors during a single frame exposure.

Even though Fourier strategy has been proven to better concentrate image energy than Hadamard (Zhang et al., 2017), it has been also shown to provide worse noise robustness. Therefore, for single pixel imaging, the first family of measurement matrix is preferable when the light efficiency is a major concern; conversely, Hadamard's is most suitable for situations in which the overall image quality is the discriminating factor.

Alongside the cited deterministic models, however, more sophisticated approaches have been proposed. In adaptive strategies, the measurement masks can be adapted to the scene as more and more features are acquired (Rousset et al., 2018; Edgar et al., 2015; Higham et al., 2018) or the information carried by the first patterns can be used as further initial condition to set up for reconstruction.

2.4. Single pixel camera for spectral and temporal measurements

In single pixel imaging the spatial information about the sample structure is intrinsically transferred from the detector array to the plane of light modulation. The capability of optically projecting the scene onto a set of preloaded measurement basis is one of the reasons beyond the success of SPCs. This method has implications, that go well beyond fluorescence microscopy, which works primarily in the visible range. Ultraviolet or IR, for example, are two spectral ranges that require expensive pixelated sensors, and cheaper alternatives are offered by CS from microscopic (Zimmermann et al., 2003), (Denk et al., 2019) to macroscopic scenery (Okhrimenko et al., 2019).

The lack of compact, efficient light sources and detectors in the spectral region spanning from 30 μm to 0.3 mm, has been the technology limit beyond the late development of imaging techniques in this range. Only in the last two decades (Ferguson and Zhang, 2002), it has been possible to build spectral (Baxter and Guglietta, 2011) or time domain imagers (Jepsen et al., 2011) in the Terahertz region. Radiation in this spectral range has many interesting properties: it can be used as testing probe for quality assessment due to its ability to penetrate many insulating materials as paper and plastic. It excites molecules vibrational modes in crystals, explosives and drugs; it can support wireless data transmission (Ishigaki et al., 2012) and it has also been used to drive electron acceleration (Nanniet al., 2015). Nonetheless, multielement image acquisition and raster scanning routines makes THz imaging inefficiently long and/or complex. Compressive imaging, based on spatial masks for THz detection is a valid alternative (Watts et al., 2014), (Chan et al., 2008).

SPC has been also successfully applied for multispectral and hyperspectral imaging, in order to reconstruct images at multiple wavelengths. The idea is to simultaneously work with different SPCs, each of them at a specific wavelength, by combining spectral detectors (e.g., linear array coupled to a dispersive element) with spatial light modulators (see Section 3) (Jin et al., 2014; Jin et al., 2016; Davis et al., 2011).

Single pixel cameras can also be coupled to time-resolved detection schemes, such as Time Correlated Single Photon Counting (TCSPC). TCSPC is a statistical method that generates a histogram of different photons arrival times, by synchronizing a train of laser pulses with single photon detection. This can provide useful insights about the sample's absorption, emission and scattering (Howland et al., 2013). In particular, fluorescence Lifetime Imaging at picosecond or nanosecond resolution finds a variety of applications spanning from biology and medicine (Marcu, 2012), (Elson et al., 2004), to material sciences (Barnard et al., 2013), (Becker, 2012), providing information about the environmental pH, temperature, polarity, and ion concentrations. In this context, CS can be used to parallelize time-resolved detection, using arrays of time-resolved detectors (Rousset et al., 2018). In addition, time resolved detection can be combined with spectral detection (Liu et al., 2019) to extract space-lifetime-spectral information together, as described in Paragraphs 3.5 and 3.6.

3. Applications of compressed sensing: from super-resolution microscopy to mesoscopy

3.1. Super-resolution microscopy

In case of individual, spatially separated fluorescent objects, it is possible to resolve the different emitters at a subwavelength resolution. In this scenario, CS can be adapted to reconstruct the sparse emitters (Gazit et al., 2010). However, when dealing with far field fluorescence microscopy, the different emitters are not well separated, and light diffraction limits the capability to resolve them. Several super-resolution techniques have been developed to address this limitation (Hell, 2007). Among them, Photo-activated localization microscopy (PALM) (Betzig et al., 2006) and STochastic Optical Reconstruction Microscopy (STORM) (Rust et al., 2006) are based on the idea of activating a limited number of fluorescent molecules in the field of view and to localize them with a precision higher than the diffraction limit.

In combination with STORM microscopy, CS is used to separate single molecules even when the emitters are not directly distinguishable: said molecules are under-sampled during the acquisition and CS offers increased localization speed by an order of magnitude (Zhu et al., 2012), (Babcock et al., 2013), (Cheng et al., 2017). In this context, Wu et al. (2018) propose the use of model-based sparse Bayesian learning, with the goal of achieving real-time image reconstruction. In alternative, a frequency domain compressed sensing technique can potentially be 1000 times faster that CS-STORM (Zhang et al., 2019). To reduce the acquisition time in single molecule localization microscopy, Li et al. (2009) propose a single-frame, wide-field nanoscopy system based on ghost imaging: a random measurement matrix composed of speckles is created with a phase modulator, which transforms the signal measurement matrix to satisfy the sparsity requirement (Li et al., 2019). The technique reconstructs a super-resolution image via sparsity constraints from one low-resolution wide-field speckle image. Furthermore, Compressed Sensing can be used in STORM microscopy to enhance three-dimensional imaging, based on novel molecules localization algorithms (Gu et al., 2014), or in combination with astigmatic imaging (Huang et al., 2015).

An alternative to PALM and STORM, is super-resolution optical fluctuation imaging (SOFI) (Dertinger et al., 2009) that from the temporal statistics of the fluorescence emissions, produces sub-diffraction images at higher temporal resolution but at cost of spatial resolution. Solomon et al. (2018) demonstrate a super-resolution microscopy technique which is based on sparsity in the correlation domain. By assuming that the blinking emitters are uncorrelated over time and space, the authors use CS to exploit the speed of SOFI at higher spatial resolution.

Structured Illumination Microscopy (SIM) (Gustafsson, 2005) has become one of the most widely used super-resolution microscopy methods. SIM is based on the projection of modulated patterns on the sample, at different spatial phases and angles. The acquisitions are combined to extend the optical transfer function of the imaging system beyond the diffraction limit. Compressed sensing can be used to reduce the number of pixels sampled and stored during the acquisition of the modulated images (Meiniel et al., 2017). Furthermore, Pascucci et al. (2019) show that speckle patterns can be used for SIM modulation and compressed reconstruction (Fig. 4a). Similarly to Li et al. (2019), the authors take advantage from the properties of speckle patterns created with a spatial light modulator. Speckles are orthogonal at different depths of propagation, maintaining high contrast. This allows the reconstruction of sparse objects in three dimensions, acquiring a single two-dimensional image. In SIM microscopy, SLM are commonly exploited to generate the illumination patters but DMDs are also widely used, even in combination with LED illumination (Dan et al., 2013). Nonetheless, the concept of SPC is not commonly used for super-resolution microscopy, but finds many applications in widefield illumination microscopy.

3.2. Wide field fluorescence microscopy

In fluorescence microscopy, one of the main issues is the low intensity of light emitted by the specimen. For this reason, in fluorescence microscopy the SPC has evolved toward a scheme where the illumination path is modulated, instead of the detection (Studer et al., 2012) (Fig. 3). Hence, in a typical fluorescence microscope based on SPC, the excitation light is modulated by a DMD and projected onto the sample. The fluorescence signal is then collected by the single pixel detector.

Some specific problems related to widefield illumination should be considered when dealing with this technique. For instance, a coherent source would produce a speckle intensity distribution which would overlap the illumination pattern. For this reason, Studer et al. (2012) insert a diffuser in the illumination path (Fig. 3b). By rotating a diffuser, speckle patterns are averaged in time during the acquisition, resulting in an effective uniform illumination. As an alternative, incoherent light can be efficiently used as source (Salvador-Balaguer et al., 2018), (Yuan and Pang, 2016). Furthermore, the area of the detector must be large enough to collect all the incoherent photons emitted by the specimen. For this reason, photomultipliers (PMT) are to be preferred over photodiodes, for their typically larger active areas. For what concerns the detection optics, the light collected from the sample should be maximized, whereas aberrations in the detection path are not a major issue. Conversely, the quality of the illumination pattern determines the achievable resolution of the system and the aberrations should be minimized in the optical system of the illumination path.

The single pixel scheme is used in many widefield-illumination microscopes, primarily with the goal to extend the capabilities of the optical system by introducing hyperspectral or time-resolved detection (see Paragraphs 3.5 and 3.6). Due to its single active element, the SPC becomes a valid candidate when designing low cost (Salvador-Balaguer et al., 2018), multimodal (Liu et al., 2018) microscopes (Fig. 4b) or when fast acquisition is needed (Guo et al., 2017). Finally, SPC finds applications in optical systems whose detection is affected by aberrations or even in presence of light diffusion between the sample and the detector (Rodríguez et al., 2014).

3.3. Optical sectioning fluorescence microscopy

In widefield fluorescence microscopy, thick specimens not only emit from the in-focus plane but from the whole illuminated volume: collecting out-of-focus light reduces the contrast and therefore the axial resolution of the acquired image. To overcome this problem, several optical sectioning techniques have been developed, aimed at collecting light only from a single specimen's plane. Among said techniques, the most widely used is confocal microscopy (Conchello and Lichtman, 2005), (Mertz, 2011), where the out-of-focus light is rejected by a pinhole placed in front of the detector in a plane conjugated with the sample. Confocal microscopy is a raster scan technique in which the illumination/detection focal spot is moved through the entire specimen in the imaging plane. Then, the depth of the imaging plane can be scanned along the axial direction. Compressed sensing offers the possibility to reduce the number of measurements, but standard confocal configurations preclude the use of modulation devices (namely a DMD). On top of this, the presence of a static pinhole in the detection is not compatible with CS reconstruction algorithms.

Nonetheless, the possibility to apply CS concepts to confocal microscopy is proposed in references (Kelly et al., 2007), (Sun et al., 2008). Ye et al. (2009) show a scheme based on randomly sparse binary masks, which are loaded on a DMD placed in the image plane of the microscope. The light reflected (or emitted) by the specimen is imaged back onto the DMD, which provides a mask to capture only in-focus light, and then, with a beam splitter (or a dichroic mirror in case of fluorescence (Wu et al., 2010)), is sent to a bucket detector. It is true that a higher degree of sparsity of the mask would result in a higher optical sectioning of the system, but it would also lead to an inefficient detection path. Within this framework, authors report the possibility to reduce the number of measurements up to 90% with respect to raster scan. Wu et al. (2010) study the optical sectioning capability of the method by using Modified Scrambled Block Hadamard Ensemble patterns. These masks are such that few "on" pixels are surrounded by "off" pixels and are sparsely distributed. The surface extension of the incoming light on the DMD, together with the mask sparsity, may imply a great reduction in the excitation power, which could limit the range of application of the technique. This is the case for multiphoton and non-linear microscopy (see next Paragraph) (Mertz, 2011). In addition, for low signal application, the masked DMD reflection of the fluorescence signal, may critically lower the system light throughput.

For these reasons, Pavillon and Smith (2016) propose a CS confocal design which keeps the laser scanning concept whilst reducing the number of measurements with a trivial subsampling of the measurement matrix. Said subsampling alone is not suitable for CS, because it does not respect the mutual incoherence between the measurement and the sparsifying matrices and may lead to reconstruction artifacts (Francis et al., 2019). Yet it is still possible to reconstruct the dataset if the imaging system (namely its point spread function, PSF) is taken into consideration. As a matter of fact, the spreading of a signal caused by the PSF implies that each measured point is the linear combination of values in the vicinity and so the PSF acts as a smoothing operator that spreads the signal contributions. The measurement matrix Φ is sparse by construction, and then Φ is applied not to x, but to the convolution between

the PSF and $\boldsymbol{x}$. The authors validated their scheme by simulations and measurements, achieving compression ratios up to 94% and an improved SNR. The main advantage of this approach is the ready application to existing laser scanning system while the ultimate compressibility is related to the PSF width. The problem of optical reconstructions from under-sampled confocal measures is also studied by Francis et al. (2019), at the regularization algorithm level. They propose an adaptive regularization method based on the image structure, that considers the maximizer of information entropy, achieving better reconstructions with respect to other methods, like multi-resolution prior-based scattered data approximation and l_1 algorithms.

An alternative approach for optical sectioning is based on Structured Illumination Microscopy (SIM). A series of light patterns is projected on the microscope's object plane and the corresponding modulated images are collected with a camera. Since in-focus and out-of-focus light are modulated differently, it is possible to reconstruct an optical section of the sample with computational methods. Furthermore, SIM is a wide-field technique, and it can provide high temporal resolution. Parot et al., 2019 use SIM with CS, to record fast neuronal activity in zebrafish. Their approach with Hadamard patterns outperforms other implementations of SIM in terms of high contrast PSF but it suffers from low time resolution. However, with compressive sensing, the authors can push the time resolution up to 500 Hz, taking advantage of the specimen features. With respect to other compressive sensing application, where spatial or temporal sparsity are enforced with adjustable parameters of iterative optimizations, the optical section estimation results from direct calculation.

3.4. Multiphoton and non linear microscopy

Multiphoton (MP) microscopy is another common paradigm to obtain optical sectioning: a light pulse, with temporal duration of about hundreds of fs, is used to cause the simultaneous absorption of two (2-photon microscopy, 2PM) or more near-infrared photons by a single fluorophore. This unlikely nonlinear event happens only at the objective's focal plane, where the intensity of the excitation light is the highest. Hence, only the fluorescence within the focal plane is excited. One major advantage of multiphoton microscopy is the use of longer wavelengths compared to visible wavelengths, resulting in a deeper penetration in scattering media, such as biological samples. For this reason, MP microscopy has opened a wide horizon of feasible biological studies (Hoover and Squier, 2013). Nonetheless, MP microscopy needs high intensities and its conventional design involves femtosecond lasers (Denk et al., 1990).

There are numerous implementations to improve the MP microscopy performances, including high speed scan systems, multimodal imaging, and multifocal excitation methods. Temporal Focusing (TF) is one of those (Oron et al., 2005) aimed at improving the acquisition speed and the sensitivity in depth (Papagiakoumou et al., 2013; Zhu et al., 2005; Rowlands et al., 2017). The technique is based on temporal broadening of ultrashort pulses and subsequent recombination of the spectral components, with the shortest pulse duration obtained only at the focal plane exploiting the dispersion properties of the sample.

Escobet-Montalbán et al. (2018) introduce a Temporal Focusing microscopy with single-pixel detection (TRAFIX). This work addresses the problem of imaging deep in diffusive tissues, taking advantage both of the TF for depth sensitivity and of the single-pixel detector for scattering robustness (Tajahuerce et al., 2014). The authors use a pulsed laser (140 fs, 80 MHz, 800 nm) and a spatial modulator (a liquid crystal on silicon) imaged onto a blazed diffraction grating to obtain pulse stretching. Specimen of different

thickness (from approximately 50 to 550 μm) are illuminated with a Hadamard basis scan. The authors present higher imaging quality and less photobleaching compared to a point scanning 2PM. Furthermore, the authors also perform a feasibility simulation for 3-photon TRAFIX (considering excitation at 1700 nm). Wijesinghe et al. (2019) demonstrate that, in TRAFIX, random patterns perform better than Hadamards, and, moreover, random Morlet basis have the additional benefit to be fully transmitted through the objective. A compression ratio up to 87.5% is achieved in imaging of beads immersed in a thick (360 μm) scattering medium (approximately $\mu'_s = 8.5$).

A similar demonstration of the technique is provided by Alemohammad et al. (2018), where a DMD is used both as diffraction grating and pattern generator, simplifying the system. In this work, the authors use pseudorandom patterns to scan fluorescent beads in a scattering medium. Additionally, they propose to use the system in a random-access imaging configuration, to target different region of interest in parallel, and then apply an adaptive sampling method to scan a subregion at finer resolution.

Multiphoton microscopy based on compressive random access is proposed by Wen et al. (2019). A holography-based technique is used to generate a multi-focus 3D scanning pattern with a DMD (Geng et al., 2017). The system exploits a femtosecond laser (200 fs, 80 MHz, and 800 nm), a DMD coupled with a grating and a photomultiplier as detector. The multi-focus random access map, which is loaded on the DMD, is generated via binary holography and a weighted Gerchberg-Saxton algorithm. The authors also discuss the possibility to perform sections not only by parallel planes, but also with arbitrary optical sectioning surfaces (e.g., parabolic, sinusoidal etc.) by properly programming the DMD.

3.5. Fluorescence Lifetime Imaging Microscopy

The information inferred from fluorescence microscopy can be significantly increased if, in addition to intensity, the fluorophore's lifetime is measured and used as an imaging parameter, as in Fluorescence Lifetime Imaging Microscopy (FLIM). In fact, the lifetime depends on de-excitation molecular processes and thus is very sensitive to the microenvironment (namely pH, temperature, intermolecular distance) and it is independent from the excitation intensity. Progresses and applications of FLIM are reported in two recent reviews (Liu et al., 2019), (Datta et al., 2020).

Conventional FLIM measurements can be performed with a raster scanning approach coupled with Time Correlated Single Photon Counting (TCSPC) detection systems. The need to both reduce the acquisition time and the data set size, led to the use of CS. In fact, the demand for fast FLIM is not only limited to the measurement process, but it also involves data processing, since lifetime estimation can be computationally heavy. A scan-less lifetime measurement system based on a coding mask, which modulates the collected light with Hadamard patterns (Hadamard Transform Imaging, HTI), is reported by Hassler et al. (2005). Mizuno and Iwata (2016) present an increment in sensitivity and time resolution, with respect to 2D gated imaging detectors (i.e., a CCD camera), by merging a method based on HTI with a Fourier-transform phase modulation fluorometer. The presented system is based on a time modulated LED matrix, and it therefore shows limited spatial and temporal resolutions. Nonetheless, the authors also propose alternatives to improve such performances, namely the use of a pulsed laser and a DMD, and a heterodyne or photon counting detection.

Outside the microscopy context, a mesoscopic compressive fluorescence lifetime imaging system is proposed by Pian et al. (2017). Their setup (Fig. 4c) involves three DMDs (enclosed in a

projection system), to provide both patterned illumination and detection, and can work in reflectance and transmittance geometry so to be adaptable to the specimen. Time-resolved signals for each pattern are recorded with a photomultiplier; additionally, a camera can be used for system calibration and reference images. This technology can be employed to perform FRET measurements *in vitro* and *in vivo*, obtaining spectrally resolved spatial maps in intensity and lifetime. The authors report a measurement time of 14 min, but they point out that with pattern optimizations (Rousset et al., 2018), (Ochoa et al., 2018), the number of measures can be further reduced. Additionally, this system can be used combined with a machine learning approach in data analysis (Yao et al., 2019).

Lifetime estimation is a non-trivial task: compressive sensing finds another possible application as a method to retrieve fluorescence parameters. Yang et al. (2015a) show that a fluorescence decay has a sparse representation, since it can be modeled as a sum of a finite number of exponentials. Hence it is well suited for compressive approaches. They model the time-resolved photon counting data from a confocal microscope as a Poisson process of unknown parameters and set the problem to retrieve such parameters with a negative Poisson log-likelihood. The sum between the latter and a l_1 norm regularization term is the objective function to be minimized, to obtain a sparse solution for the amplitudes and lifetimes, by means of CS. This approach shows to be more robust for low photon counts with respect to other techniques, i.e., non-linear least squares fitting, fast fitting and maximum likelihood.

Recent developments in FLIM include the field of compressed ultrafast photography (CUP) (Gao et al., 2014). Thompson et al. (2017) were the first to report the possibility to acquire an entire fluorescent lifetime image with a single laser pulse, directly on cells, by means of a streak camera. The main benefit of CUP is that complex and fast biological events can be seen with a one-shot acquisition, unlike the more common ultrafast optical techniques (e.g., pump-probe and up-conversion) for the study of ultra-fast phenomena. Wang et al. (2020) demonstrate a single-shot spectrally resolved FLIM. In their system (Fig. 5b), the light from the specimen is split into two paths: the first leading to a camera while the second to a DMD which reflects light onto a streak camera. CS is applied to retrieve a time and spectrum resolved image from the data collected within the two paths. Finally, the frame rate depends on the sweeping speed of the streak tube and the camera's pixel size, while the temporal information is retrieved with a single shot. Despite samples are markers in cuvettes, preprints are reporting that the technique is starting to be applied even *in vivo* in cells (Ma et al., 2020).

3.6. Hyperspectral microscopy

Another possibility to enrich a fluorescence microscopy dataset is to perform spectral imaging. This strategy is used to identify spectrally overlapping emitters or to isolate markers from an autofluorescent background, with the goal to collect structural and functional information from cells, tissues, interacting proteins. As a matter of fact, the spectrum is sensitive to the local microenvironment, similarly as the lifetime. Spectrally resolved microscopy is employed, among others, in cellular imaging, gene mapping, and pathology (Gao and Smith, 2015). The literature reports a distinction between two spectral domains: imaging is called *multispectral* when the spectral resolution is > 10 *nm* and the dataset in made of 3 to 10 normally spaced spectral bands. It is called *hyperspectral* when the resolution is below 10 *nm*, from tens to hundreds of nanometers wide bands.

Spectral measurements at high resolution require longer acquisition time, which could be reduced with CS. The coded aperture snapshot spectral imager (CASSI) discussed by Cull et al. (2010), is a pioneer design to apply CS to fluorescence microscopy. Said imager (Fig. 5a), is a prism-based system which can be cascaded to a commercial fluorescence microscope. The collected light is spectrally dispersed along one spatial dimension, then a spatial modulation is applied to the sheared data, and finally the spectral components are recombined. The data cube (x, y, λ) is detected by a camera within a single shot. The dataset cube is retrieved with a Two-step Iterative Shrinkage/Thresholding (TwIST) algorithm with the total variation minimization.

An alternative technique is the compressed ultrafast spectral photography (CUSP) presented by Wang et al. (2020) and already discussed in the previous paragraph. According to this design (Fig. 5b), spectral detection is achieved with a diffraction grating
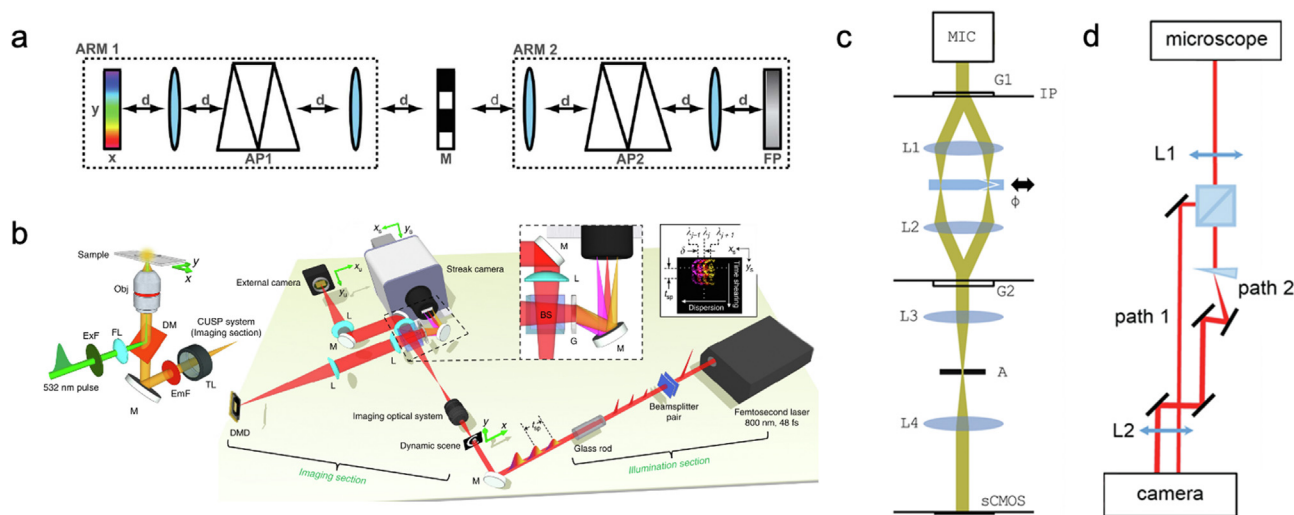

Fig. 5. Four different methods to perform a spectrally resolved compressive fluorescence microscopy: (a) CASSI, reprinted with permission from (Cull et al., 2010) © The Optical Society; (b) CUSP. Left: illumination section for the microscope. Right: complete CUSP setup. Adapted from (Wang et al., 2020) under a Creative Commons Attribution 4.0 International License (http://creativecommons.org/licenses/by/4.0/), (c) IFTS, adapted with permission from (Wadduwage et al., 2017) © The Optical Society; here two diffraction gratings (G1 and G2) generate the interferometer and a variation of the thickness of a glass block is used to introduce a path length difference. An aperture (A) is introduced to block off-axis orders. (d) Space-constrained computational spectral imaging detection system. Adapted with permission from (Wang et al., 2019) © The Optical Society.

(G) that spatially disperses the fluorescence signal on the streak camera. In such a way, the sweep of the streak camera detects the time, the spatial position the spectrum, and the image is encoded with a pattern projected on a DMD. The reconstruction is again obtained using the TwIST algorithm.

The use of CS with SPC for hyperspectral imaging is originally discussed in Studer et al. (2012) (Fig. 3b): a spectrometer coupled to a linear Electron-multiplying CCD camera, provides nanometer spectral resolution. A series of Hadamard patterns is used to encode the data cube. The reconstruction can be obtained either by independently considering the spectral bands or the intrinsic nature of the data, which is sparser in spectrum than in space. In this way, the authors apply a compression ratio of 97% (and up to 99%, but with some information loss) in space and reconstruct the spectral information at a compression ratio of 98%, with some distortions in the low intensity part of the spectrum. As optimization, the authors propose a sampling strategy that acquires information in the low and in the high part of the power spectrum. Pian et al. (2017) use a commercial Czerny-Turner spectrometer coupled with a PMT detector (Fig. 4c) in a SPC scheme.

Another class of spectral resolved schemes is based on interferometric methods, namely the Imaging Fourier transform spectrometry (IFTS). In IFTS, the signal collected by each point of the specimen is split in two and sent to an interferometer. A pathlength difference is introduced between the two arms of the interferometer, generating an interference figure at the detector. The interferogram is recorded with a camera and the data cube is retrieved with an inverse Fourier transform. One advantage of the interferometric design is that the spectral bandwidth and resolution are tunable according to the path length differences. CS can be applied to reduce the number of samples in the interferogram to be acquired. However, it is crucial that the system outputs a uniform phase difference across the entire field of view. An intrinsically more stable design is IFTS based on a common path interferometer (Candeo et al., 2019). Wadduwageet al. (2017) propose a nearly common path IFTS, where the light is processed by the same optical components except for a glass block. The system is drawn in Fig. 5c. To apply CS, the optical phase can be varied either randomly or in an optimized way. The IFTS approach is also implemented by Moshtaghpour et al. (2019). This work reduces the light exposure and optimizes the path difference scan, by keeping the photon budget and spectral resolution fixed. The authors discuss two illumination schemes based on temporal and spatial modulation.

Finally, Wang et al. (2019) propose a computational spectral imaging strategy, where the spatial information from fluorescence is used as a constraint for the multispectral reconstruction. The specimen is illuminated with multiple randomly coded patterns. Then, in the collection arm, half of the light leads directly to a camera, the other is spectrally dispersed through a wedge, and is then imaged in a different area of the same camera. With distinct spectra, a 5 Hz frame rate is achieved.

3.7. Light sheet microscopy

Light Sheet Fluorescent Microscopy (LSFM) is a microscopy technique in which excitation light is confined over a single plane (light sheet) and the emitted fluorescence signal is collected on an orthogonal path with a widefield detector (Huisken, 2004). This design comes with intrinsic optical sectioning capability, together with high-speed volumetric acquisition rate and low phototoxicity, which makes it a suitable tool for volumetric, time-lapse measurements (Olarte et al., 2018). Together with Optical Projection Tomography (Correia et al., 2015), LSFM is a powerful technique to image living embryos and large mm-scaled chemically cleared biological samples.

An alternative to light sheet illumination consists in illuminating a volume of the sample modulated along the detection direction of the microscope (i.e., the axial direction of the microscope). This can be obtained by modulating the light intensity while the light sheet is scanned axially through the sample (Woringer et al., 2017) or projecting light patterns (e.g., with a DMD) modulated along the axial direction (Calisesi et al., 2019). We call this second method spatially modulated Selected Volume Illumination Microscopy (smSVIM), which is also described in Fig. 6. In both cases, the light collected by each pixel of the detector is the integral of the product between the illumination pattern and the fluorescence distribution along the axial direction.

For each pixel position (i, j), the described situation is formally equivalent to:

$$y_{(i, j)} = \Phi \cdot x_{(i, j)} \tag{3.1}$$

where $\boldsymbol{y}_{(i,j)}$ is the column vector of the intensities y_m per each pixel position, Φ is the overall measurement set, whose rows are the basis measurement functions and $\boldsymbol{x}_{(i,j)}$ is the fluorescence concentration profile along the axial direction, specified by the n-axis, at the position (i, j). This reconstructs the depth information along z, on the direction perpendicular to the detection. Let us assume to create the modulation with a DMD, as in a smSVIM setup. The Walsh-Hadamard basis is the one of choice, due to its compatibility with fast DMD modulation and to its 50% fill factor. If $M = N$ frames are acquired, it is possible to reconstruct the fluorescence profile, corresponding to n sections of the volume, by solving a well-posed inverse problem, similarly to what done in single-pixel camera applications. One advantage in using smSVIM, over LSFM, is given by the possibility to use CS. Here, CS is used to reduce the number M of patterns projected on the sample to a number smaller than the number of reconstructed planes N (the number of acquisitions that would be required in LSFM). In this way the fluorescence bleaching and the measurement time can be reduced (Calisesi et al., 2019).

3.8. Small animal imaging

Due to the large availability of fluorescent proteins and probes, many different functional processes can be monitored in living animals (Ntziachristos, 2006), (Weissleder and Ntziachristos, 2003). When dealing with thick biological tissues, the light enters in a diffusive (or scattering) regime, thus strongly limiting the achievable spatial resolution. Light propagating in a typical biological tissue experiences a mean-free path of about 100 μm (corresponding to a reduced scattering coefficient $\mu'_s = 10 \, cm^{-1}$ with anisotropy factor $g = 0.9$) (Jacques, 2013). This means that a dedicated model of its propagation in the medium is needed for recovering the spatial distribution of the fluorescence inside the volume.

The typical configuration for fluorescence imaging in the macroscopic scale is depicted in Fig. 7. The sample is illuminated with light which can be modulated in space or time. After injection, the light propagating in the sample is scattered, absorbed, and eventually excites fluorescence due to localized fluorescent markers. In turn, this emitted light will propagate again under a diffusive regime and will eventually be detected on the surface of the sample. The aim is to recover the fluorescence distribution inside the sample from the measurements performed at the boundary. This technique is called Fluorescence Molecular Tomography (FMT), or Fluorescence Diffuse Optical Tomography (FDOT) (Arridge and Schotland, 2009), (Darne et al., 2014). FDOT problem is generally faced by calculating a *Sensitivity matrix (or Jacobian matrix)*, which represents the change in the detected fluorescence
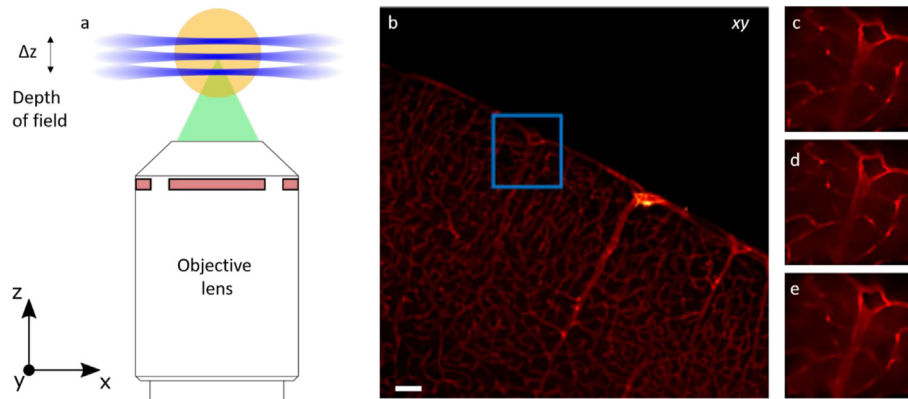
Fig. 6. Schematics of smSVIM (a). Reconstruction of a chemically cleared biological sample, mouse brain labelled with Cy 5 (b) at different compression ratios, namely CR = 50% (c), CR = 75% (d) and CR = 87.5% (e), scale bar is 1 mm.
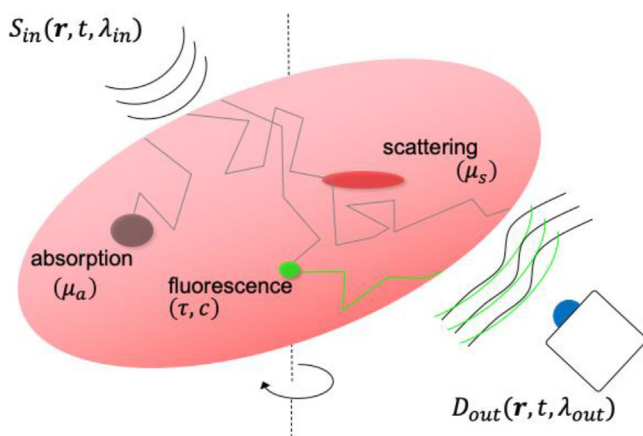

Fig. 7. Measurement scheme in Fluorescence Diffuse Optical Tomography.

signal due to a small change of the yield in each voxel of the sample (Arridge, 1995), (Arridge and Schweiger, 1995). It is worth noting that under the assumption of known optical properties, at both the excitation and emission wavelength, the problem becomes linear with respect to the fluorescence yields, while the general problem of Diffuse Optical Tomography is intrinsically nonlinear (Arridge and Schotland, 2009), (Darne et al., 2014). To construct this matrix, a proper model of the light-propagation from the source to the detectors and inside the tissue is required. At this purpose, numerical methods based on finite-elements (FEM) (Arridge et al., 1993) or fast Monte-Carlo (MC) simulations (Fang and Boas, 2009), (Yao et al., 2016) can be used. These methods are suitable for complex geometries like small animals, namely a mouse.

Once the *sensitivity matrix* is computed, the problem can be formulated as in Eq. (1.1) where Φ is the sensitivity matrix, $\boldsymbol{y}$ is the measurements vector and $\boldsymbol{x}$ is the unknown fluorescence amplitude for each voxel. The problem is ill-posed because it is underdetermined (Arridge and Schotland, 2009), (Arridge, 1999), and regularization is required. Thus, the solution is typically obtained by solving the optimization problem in Eq. (1.3): where τ is the regularization parameter and $\mathscr{R}(\boldsymbol{x})$ is a regularization functional (or prior) which can be selected to drive the solution towards a certain characteristic, such as sparsity in some domain, smoothing, etc. (Correia et al., 2011).

Pioneering works on FDOT (Ntziachristos, 2006), (Weissleder and Ntziachristos, 2003) use dense point-like illumination and detections, with a high complexity of the setup. The initial idea was

to cover the surface as much as possible with illumination/detection points to maximize the spatial resolution. For each injection point all detectors were activated, thus generating a big quantity of data. In this framework different compression strategies were proposed, paving the way to the application of CS in fluorescence molecular imaging of small animals.

The first proposed compression strategies rely on data compression after measurement. The typical setup consists of a point-source (usually a laser) for illumination and a CCD for detection. Each pixel acts as a single point-like detector so that the sensitivity matrix has to be constructed considering all the source-detectors combinations. Moreover, considering the possibility of a moving source, the number of combinations critically increases. Considering that a biological tissue acts as a low-pass filter (Bassi et al., 2008), the majority of the acquired images are compressible in the Fourier space, thus allowing their storage with limited Fourier coefficients. This approach is pursued by Ripoll (2010) under a simple geometry of slab, for which the sensitivity matrix can be analytically computed, due to the concise Fourier representation of the point-like source/detection combination.

A similar approach is proposed by Rudge et al. (2010). In this case the compression is performed in the wavelet-basis: the wavelet-transform is applied to the CCD images, the coefficients with smaller weights are filtered and the inversion is performed in the wavelet-space. This filtering strongly reduces the number of rows in the sensitivity matrix. Moreover, they use a FEM approach which suites the application to a realistic small animal model.

The development of spatial light modulators, and particularly DMDs, has made spatial light modulation straightforward both in illumination and detection. An extensive use of structured illumination has been applied by Ducros et al. (D'Andrea et al., 2010; Ducros et al., 2010; Ducros et al., 2012; Ducros et al., 2013; Ducros et al., 2016): in these works, the authors investigate different illumination patterns, ranging from Fourier to Haar wavelet basis, coupled to a CCD acquisition. More details on the use of structured illumination in biomedical imaging can be found elsewhere (Angelo et al., 2018). The increasing availability of spatial light modulators allowed the implementation of the single-pixel camera in the field of macroscopic optical imaging. This approach paved the way both to the development of advanced compression strategies and to multi-dimensional imaging (space, wavelength, time): the possibility of shrinking the space dimension into a single-detector (either compressed or not) allows one to explore other dimensions with time- and/or space-resolved detectors. As an example, Pian et al. (2017) report a system based on two DMDs, one for illumination and the other one for detection, resolving in time,

space and wavelength, the fluorescence in Förster Resonance Energy Transfer (FRET) experiments. Moreover, thanks to the availability of programmable masks, strategies for data-driven adaptation of the measurement have been developed. As an example, Rousset et al. (2018) propose an adaptive strategy for reducing up to a compression ratio of 93% the measurements performed on a fluorescent sample, to obtain a hypercube data with space, time and emission spectrum. An exhaustive comparison of different illumination patterns, compressions and solvers is discussed by Ochoa et al. (2018).

Since the dimensionality of the measurement space is smaller than that of the volume distribution of the fluorophores, the problem formulated by FDOT is intrinsically ill-posed. Yet, in many small animal imaging experiments, what we want to recover are the localized distribution of the fluorescence signal. This means that the searched signal is locally zero almost everywhere. By introducing a proper penalty term $\mathscr{R}(\boldsymbol{x})$ (such as l_1 minimization, described in Section 1), it is possible to promote sparsity in the solution, obtaining sharper and more accurate reconstructions. This approach has been pursued by different research groups (Zhao et al., 2014; Yang et al., 2018; Zhu and Li, 2014) with improved reconstruction quality compared to classical l_2-based methods. In particular, the following works are remarkable: (Yang et al., 2015b) which proposes the use of the l_1-norm of the Fourier-transform solution (Zhao et al., 2014), which introduces a general l_p-norm terms and compare reconstructions with $p = \{1/16, 1/4, 1, 2\}$, and lastly (Zhu and Li, 2014), which compares different regularization terms based on 3 different norms.

Due to the promising results given by sparse-reconstruction, CS has been widely used for the optimization of the sampling strategy in FDOT, by exploring the incoherence of the sensitivity matrix. Jin et al. (2012) propose a method to construct preconditioners for the sensitivity matrix aiming at reducing its coherence. The sensitivity matrix W in CW-FDOT is the column-wise Kronecker product of two matrices: the excitation field Φ, and the emission field G. By reducing their coherence through proper preconditioners, it is possible to reduce the coherence of W as well, thus improving the quality of sparse reconstructions. The formulation of the two preconditioners is equivalent to the calculation of optimal illumination and detection masks. The experimental configuration is based on different point sources and a CCD camera. The preconditioners are calculated *a-posteriori* and applied before the reconstruction.

Yang and Yao (Yao et al., 2015), (Yang et al., 2018) implement this approach in a setup based on a two-DMDs configuration, both in illumination and detection, paired with a proper sparse-reconstruction algorithm. The optimal illumination and detection patterns are precomputed and loaded on the DMD during the measurements, thus reducing the acquisition time whilst maintaining the information content. The pre-computation of the optimal patterns is possible under the assumption that medium optical properties at both excitation and emission wavelengths are known and do not vary during the experiment.

Overall CS in small animal imaging has been used both for deriving sensing strategies (illumination and detection) to be implemented in an experimental system and for reconstruction of sparse signals. It is worth noting that, differently from other applications, the cited *sensitivity matrix* differs from a *sensing* matrix since the input and output are decoupled by the scattering medium: the projected pattern is not preserved inside the volume, but it is distorted by the diffusion of light. Consequently, a double-DMD configuration is typically required for implementing CS strategies (Farina et al., 2017).

4. Conclusions

First proposed in 2006, compressed sensing techniques have since been steadily increasing in terms of rate of theoretical development and applications. In the field of fluorescence microscopy, CS facilitates image reconstruction with a reduced amount of acquired data, potentially speeding up measurement routines. Furthermore, CS is at the basis of the development of single-pixel camera methods. This technique is widely used in fluorescence imaging, illuminating the sample with structured light, and collecting the emitted fluorescence with a bucket detector. Coupled with spectral and time-resolved detection, the single pixel camera is a valuable option to achieve hyperspectral and fluorescence lifetime imaging. Nonetheless, for its general mathematical framework, CS algorithms are widely and successfully used in optical imaging at multiple spatial scales, from super-resolution microscopy to mesoscopic imaging of small animals.

Author contribution

D.A. wrote the first chapter, G.C. the second, A.B, G.C, A.G. and A.F. the third and fourth chapters. All the authors contributed and proof-read the whole article. A.B. supervised the work.

Declaration of competing interest

The authors declare no conflict of interest.

Acknowledgements

References

Alemohammad, M., et al., 2018. Widefield compressive multiphoton microscopy. Opt. Lett. 43 (12), 2989. https://doi.org/10.1364/ol.43.002989.

Ancora, D., Leuzzi, L., 2019. Transmission Matrix Inference via Pseudolikelihood Decimation. " *arXiv*, pp. 1—35.

Angelo, J.P., Chen, S.-J.K., Ochoa, M., Sunar, U., Gioux, S., Intes, X., 2018. Review of structured light in diffuse optical imaging. J. Biomed. Opt. 24, 1. https://doi.org/10.1117/1.jbo.24.7.071602, 07.

Arridge, S.R., 1995. Photon-measurement density functions Part I: analytical forms. Appl. Opt. 34 (31), 7395. https://doi.org/10.1364/ao.34.007395.

Arridge, S.R., Apr. 1999. Optical tomography in medical imaging. Inverse Probl. 15 (2), R41—R93. https://doi.org/10.1088/0266-5611/15/2/022.

Arridge, S.R., Schotland, J.C., Dec. 2009. Optical tomography: forward and inverse problems. Inverse Probl. 25 (12), 123010. https://doi.org/10.1088/0266-5611/25/12/123010.

Arridge, S.R., Schweiger, M., Dec. 1995. Photon-measurement density functions Part 2: finite-element-method calculations. Appl. Opt. 34 (34), 8026. https://doi.org/10.1364/AO.34.008026.

Arridge, S.R., Schweiger, M., Hiraoka, M., Delpy, D.T., 1993. A finite element approach for modeling photon transport in tissue. Med. Phys. 20 (2), 299—309.

Babcock, H.P., Moffitt, J.R., Cao, Y., Zhuang, X., 2013. Fast compressed sensing analysis for superresolution imaging using L1-homotopy. Opt Express 21 (23), 28583—28596. https://doi.org/10.1364/OE.21.028583.

Baraniuk, R., Jul. 2007. Compressive sensing [lecture notes]. IEEE Signal Process. Mag. 24 (4), 118—121. https://doi.org/10.1109/MSP.2007.4286571.

Baraniuk, R., Steeghs, P., Apr. 2007. Compressive radar imaging. In: IEEE National Radar Conference - Proceedings, pp. 128—133. https://doi.org/10.1109/RADAR.2007.374203.

Barnard, E.S., et al., Dec. 2013. Probing carrier lifetimes in photovoltaic materials using subsurface two-photon microscopy. Sci. Rep. 3 (1), 2098. https://doi.org/10.1038/srep02098.

Bassi, A., D'Andrea, C., Valentini, G., Cubeddu, R., Arridge, S., 2008. Temporal propagation of spatial information in turbid media. Opt. Lett. 33 (23), 2836. https://doi.org/10.1364/ol.33.002836.

Baxter, J.B., Guglietta, G.W., Jun. 2011. Terahertz spectroscopy. Anal. Chem. 83 (12), 4342—4368. https://doi.org/10.1021/ac200907z.

Becker, W., 2012. Fluorescence lifetime imaging - techniques and applications. J. Microsc. 247 (2), 119—136. https://doi.org/10.1111/j.1365-2818.2012.03618.x.

Betzig, E., et al., 2006. Imaging intracellular fluorescent proteins at nanometer resolution. Science 313 (5793), 1642—1645. https://doi.org/10.1126/science.1127344 (80-.).

Bishara, W., Su, T.-W., Coskun, A.F., Ozcan, A., May 2010. Lensfree on-chip microscopy over a wide field-of-view using pixel super-resolution. Opt Express 18 (11), 11181. https://doi.org/10.1364/oe.18.011181.

Calisesi, G., et al., Nov. 2019. Spatially modulated illumination allows for light sheet fluorescence microscopy with an incoherent source and compressive sensing. Biomed. Opt Express 10 (11), 5776. https://doi.org/10.1364/BOE.10.005776.

Candeo, A., et al., Dec. 2019. A hyperspectral microscope based on an ultrastable common-path interferometer. APL Photonics 4 (12), 120802. https://doi.org/10.1063/1.5129860.

Candès, E., Romberg, J., Jun. 2007. Sparsity and incoherence in compressive sampling. Inverse Probl. 23 (3), 969—985. https://doi.org/10.1088/0266-5611/23/3/008.

Candes, E.J., Tao, T., Dec. 2006. Near-optimal signal recovery from random projections: universal encoding strategies? IEEE Trans. Inf. Theor. 52 (12), 5406—5425. https://doi.org/10.1109/TIT.2006.885507.

Candes, E.J., Wakin, M.B., 2008. An introduction to compressive sampling: a sensing/sampling paradigm that goes against the common knowledge in data acquisition. IEEE Signal Process. Mag. 25 (2), 21—30. https://doi.org/10.1109/MSP.2007.914731.

Candès, E.J., Romberg, J.K., Tao, T., Aug. 2006. Stable signal recovery from incomplete and inaccurate measurements. Commun. Pure Appl. Math. 59 (8), 1207—1223. https://doi.org/10.1002/cpa.20124.

Chan, W.L., Charan, K., Takhar, D., Kelly, K.F., Baraniuk, R.G., Mittleman, D.M., Sep. 2008. A single-pixel terahertz imaging system based on compressed sensing. Appl. Phys. Lett. 93 (12), 121105. https://doi.org/10.1063/1.2989126.

Chen, S.S., Donoho, D.L., Saunders, M.A., 2001. Atomic Decomposition by Basis Pursuit.

Chen, G.H., Tang, J., Leng, S., Jan. 2008. Prior image constrained compressed sensing (PICCS): a method to accurately reconstruct dynamic CT images from highly undersampled projection data sets. Med. Phys. 35 (2), 660—663. https://doi.org/10.1118/1.2836423.

Chen, Z., Basarab, A., Kouame, D., Mar. 2016. Compressive deconvolution in medical ultrasound imaging. IEEE Trans. Med. Imag. 35 (3), 728—737. https://doi.org/10.1109/TMI.2015.2493241.

Cheng, T., Chen, D., Yu, B., Niu, H., May 2017. Reconstruction of super-resolution STORM images using compressed sensing based on low-resolution raw images and interpolation. Biomed. Opt Express 8 (5), 2445. https://doi.org/10.1364/BOE.8.002445.

Coifman, R., Geshwind, F., Meyer, Y., Jan. 2001. Noiselets. Appl. Comput. Harmon. Anal. 10 (1), 27—44. https://doi.org/10.1006/acha.2000.0313.

Conchello, J.-A., Lichtman, J.W., 2005. Optical sectioning microscopy. Nat. Methods 2 (12), 920—931. https://doi.org/10.1038/nmeth815.

Correia, T., et al., Sep. 2011. Split operator method for fluorescence diffuse optical tomography using anisotropic diffusion regularisation with prior anatomical information. Biomed. Opt Express 2 (9), 2632. https://doi.org/10.1364/BOE.2.002632.

Correia, T., et al., Aug. 2015. Accelerated optical projection tomography applied to in vivo imaging of zebrafish. PloS One 10 (8), e0136213. https://doi.org/10.1371/journal.pone.0136213.

Cull, C.F., Choi, K., Brady, D.J., Oliver, T., Apr. 2010. Identification of fluorescent beads using a coded aperture snapshot spectral imager. Appl. Opt. 49 (10), B59. https://doi.org/10.1364/AO.49.000B59.

Dan, D., et al., Dec. 2013. DMD-based LED-illumination Super-resolution and optical sectioning microscopy. Sci. Rep. 3 (1), 1116. https://doi.org/10.1038/srep01116.

Darne, C., Lu, Y., Sevick-Muraca, E.M., Jan. 2014. Small animal fluorescence and bioluminescence tomography: a review of approaches, algorithms and technology update. Phys. Med. Biol. 59 (1), R1—R64. https://doi.org/10.1088/0031-9155/59/1/R1.

Datta, R., Heaster, T.M., Sharick, J.T., Gillette, A.A., Skala, M.C., May 2020. Fluorescence lifetime imaging microscopy: fundamentals and advances in instrumentation, analysis, and applications. J. Biomed. Opt. 25, 1. https://doi.org/10.1117/1.JBO.25.7.071203, 07.

Davis, B.M., Hemphill, A.J., Cebeci Maltas, D., Zipper, M.A., Wang, P., Ben-Amotz, D., Jul. 2011. Multivariate hyperspectral Raman imaging using compressive detection. Anal. Chem. 83 (13), 5086—5092. https://doi.org/10.1021/ac103259v.

Denk, W., Strickler, J.H., Webb, W.W., 1990. Two-photon laser scanning fluorescence microscopy. Science (80-.) 248 (4951), 73—76. https://doi.org/10.1126/science.2321027.

Denk, O., Musiienko, A., Žídek, K., 2019. Differential single-pixel camera enabling low-cost microscopy in near-infrared spectral region. Opt Express 27 (4), 4562. https://doi.org/10.1364/oe.27.004562.

Dertinger, T., Colyer, R., Iyer, G., Weiss, S., Enderlein, J., Dec. 2009. Fast, background-free, 3D super-resolution optical fluctuation imaging (SOFI). Proc. Natl. Acad. Sci. Unit. States Am. 106 (52), 22287—22292. https://doi.org/10.1073/pnas.0907866106.

Donoho, D.L., Apr. 2006. Compressed sensing. IEEE Trans. Inf. Theor. 52 (4), 1289—1306. https://doi.org/10.1109/TIT.2006.871582.

Donoho, D.L., Huo, X., 2001. Uncertainty principles and ideal atomic decomposition. IEEE Trans. Inf. Theor. 47 (7), 2845—2862. https://doi.org/10.1109/18.959265.

Donoho, D., Tanner, J., Nov. 2009. Observed universality of phase transitions in high-dimensional geometry, with implications for modern data analysis and signal processing. Philos. Trans. R. Soc. A Math. Phys. Eng. Sci. 367 (1906), 4273—4293. https://doi.org/10.1098/rsta.2009.0152.

Duarte, M.F., et al., Mar. 2008. Single-pixel imaging via compressive sampling. IEEE Signal Process. Mag. 25 (2), 83—91. https://doi.org/10.1109/MSP.2007.914730.

Ducros, N., D'andrea, C., Valentini, G., Rudge, T., Arridge, S., Bassi, A., 2010. Full-wavelet approach for fluorescence diffuse optical tomography with structured illumination. Opt. Lett. 35 (21), 3676. https://doi.org/10.1364/ol.35.003676.

Ducros, N., D'Andrea, C., Bassi, A., Valentini, G., Arridge, S., Jun. 2012. A virtual source pattern method for fluorescence tomography with structured light. Phys. Med. Biol. 57 (12), 3811—3832. https://doi.org/10.1088/0031-9155/57/12/3811.

Ducros, N., Bassi, A., Valentini, G., Canti, G., Arridge, S., D'Andrea, C., Jan. 2013. Fluorescence molecular tomography of an animal model using structured light rotating view acquisition. J. Biomed. Opt. 18 (2), 020503 https://doi.org/10.1117/1.JBO.18.2.020503.

Ducros, N., Correia, T., Bassi, A., Valentini, G., Arridge, S., D'Andrea, C., Oct. 2016. Reconstruction of an optical inhomogeneity map improves fluorescence diffuse optical imaging. Biomed. Phys. Eng. Express 2 (5), 055020. https://doi.org/10.1088/2057-1976/2/5/055020.

Dudley, D., Duncan, W.M., Slaughter, J., Jan. 2003. Emerging digital micromirror device (DMD) applications. In: MOEMS Display and Imaging Systems, vol. 4985, p. 14. https://doi.org/10.1117/12.480761.

D'Andrea, C., Ducros, N., Bassi, A., Arridge, S., Valentini, G., Sep. 2010. Fast 3D optical reconstruction in turbid media using spatially modulated light. Biomed. Opt Express 1 (2), 471. https://doi.org/10.1364/BOE.1.000471.

Edgar, M.P., Gibson, G.M., Padgett, M.J., 2019. Principles and prospects for single-pixel imaging. Nat. Photonics. https://doi.org/10.1038/s41566-018-0300-7.

Edgar, M.P., Sun, M.-J., Gibson, G.M., Spalding, G.C., Phillips, D.B., Padgett, M.J., Sep. 2016. Real-time 3D video utilizing a compressed sensing time-of-flight single-pixel camera. In: Optical Trapping and Optical Micromanipulation XIII, vol. 9922, p. 99221B. https://doi.org/10.1117/12.2239113.

Edgar, M.P., et al., Sep. 2015. Simultaneous real-time visible and infrared video with single-pixel detectors. Sci. Rep. 5 (1), 10669. https://doi.org/10.1038/srep10669.

Elson, D., et al., 2004. Time-domain fluorescence lifetime imaging applied to biological tissue. Photochem. Photobiol. Sci. 3 (8), 795—801. https://doi.org/10.1039/b316456j.

Escobet-Montalbán, A., et al., Dec. 2018. Wide-field multiphoton imaging through scattering media without correction. Sci. Adv. 4 (10), eaau1338. https://doi.org/10.1126/sciadv.aau1338.

Fang, Q., Boas, D.A., 2009. Monte Carlo simulation of photon migration in 3D turbid media accelerated by graphics processing units. Opt Express 17 (22), 20178. https://doi.org/10.1364/oe.17.020178.

Farina, A., et al., 2017. Multiple-view diffuse optical tomography system based on time-domain compressive measurements. Opt. Lett. 42 (14), 2822. https://doi.org/10.1364/ol.42.002822.

Feng, L., Benkert, T., Block, K.T., Sodickson, D.K., Otazo, R., Chandarana, H., Apr. 2017. Compressed sensing for body MRI. J. Magn. Reson. Imag. 45 (4), 966—987. https://doi.org/10.1002/jmri.25547.

Ferguson, B., Zhang, X.-C., 2002. Materials for terahertz science and technology. Nat. Mater. 1 (1), 26—33. https://doi.org/10.1038/nmat708, 9.

Figueiredo, M.A.T., Nowak, R.D., Wright, S.J., Dec. 2007. Gradient projection for sparse reconstruction: application to compressed sensing and other inverse problems. IEEE J. Sel. Top. Signal Process. 1 (4), 586—597. https://doi.org/10.1109/JSTSP.2007.910281.

Francis, B., Mathew, M., Arigovindan, M., Jul. 2019. Image reconstruction from undersampled confocal microscopy data using multiresolution based maximum entropy regularization. J. Instrum. 14 https://doi.org/10.1088/1748-0221/14/07/P07015, 07, pp. P07015—P07015.

Gao, L., Smith, R.T., 2015. "Optical hyperspectral imaging in microscopy and spectroscopy — a review of data acquisition. J. Biophot. 8 (6), 441—456. https://doi.org/10.1002/jbio.201400051.

Gao, L., Liang, J., Li, C., Wang, L.V., 2014. Single-shot compressed ultrafast photography at one hundred billion frames per second. Nature 516 (729), 74—77. https://doi.org/10.1038/nature14005.

Gazit, S., Szameit, A., Eldar, Y.C., Segev, M., 2010. Super-resolution and reconstruction of sparse sub-wavelength images: erratum. Opt Express 18 (25), 26631. https://doi.org/10.1364/oe.18.026631.

Geadah and Corinthios, May 1977. Natural, dyadic, and sequency order algorithms and processors for the Walsh-Hadamard transform. IEEE Trans. Comput. C—26 (5), 435—442. https://doi.org/10.1109/TC.1977.1674860.

Geng, Q., Gu, C., Cheng, J., Chen, S., 2017. Digital micromirror device-based two-photon microscopy for three-dimensional and random-access imaging. Optica 4 (6), 674. https://doi.org/10.1364/optica.4.000674.

Gu, L., et al., Jun. 2014. High-Density 3D single molecular analysis based on compressed sensing. Biophys. J. 106 (11), 2443—2449. https://doi.org/10.1016/j.bpj.2014.04.021.

Guo, Q., Chen, H., Weng, Z., Chen, M., Yang, S., Xie, S., 2015. Compressive sensing based high-speed time-stretch optical microscopy for two-dimensional image acquisition. Opt Express 23 (23), 29639. https://doi.org/10.1364/oe.23.029639.

Guo, Q., et al., Feb. 2017. High-speed compressive microscopy of flowing cells using sinusoidal illumination patterns. IEEE Photonics J. 9 (1), 1—11. https://doi.org/10.1109/JPHOT.2016.2644869.

Gustafsson, M.G.L., 2000. Surpassing the lateral resolution limit by a factor of two using structured illumination microscopy. J. Microsc. 198 (2), 82—87. https://doi.org/10.1046/j.1365-2818.2000.00710.x.

Gustafsson, M.G.L., Sep. 2005. Nonlinear structured-illumination microscopy: wide-field fluorescence imaging with theoretically unlimited resolution. Proc. Natl. Acad. Sci. Unit. States Am. 102 (37), 13081–13086. https://doi.org/10.1073/pnas.0406877102.

Hager, W.W.W.W., Zhang, H., 2006. A survey of nonlinear conjugate gradient methods. Pacific J. Optim. 2 (1), 35–58 [Online]. Available: http://www.ybook.co.jp/online2/oppjo/vol2/p35.html%5Cnhttp://www.math.ufl.edu/~hager/papers/CG/%5Cnhttp://www.math.lsu.edu/~hozhang/papers/cgsurvey.pdf.

Harwit, Martin, Neil, J., Sloane, A., 1979. Hadamard Transform Optics. Elsevier.

Hassler, K., Anhut, T., Lasser, T., Dec. 2005. Time-resolved Hadamard fluorescence imaging. Appl. Opt. 44 (35), 7564–7572. https://doi.org/10.1364/AO.44.007564.

Hastie, T., Tibshirani, M.R., Wainwright, H., 2015. Statistical Learning with Sparsity: the Lasso and Generalizations. CRC press.

Hell, S.W., May 2007. Far-field optical nanoscopy. Science 316 (5828), 1153–1158. https://doi.org/10.1126/science.1137395 (80-.).

Higham, C.F., Murray-Smith, R., Padgett, M.J., Edgar, M.P., Dec. 2018. Deep learning for real-time single-pixel video. Sci. Rep. 8 (1), 2369. https://doi.org/10.1038/s41598-018-20521-y.

Hoover, E.E., Squier, J.A., 2013. Advances in multiphoton microscopy technology. Nat. Photonics 7 (2), 93–101. https://doi.org/10.1038/nphoton.2012.361.

Howland, G.A., Lum, D.J., Ware, M.R., Howell, J.C., 2013. Photon counting compressive depth mapping. Opt Express 21 (20), 23822. https://doi.org/10.1364/oe.21.023822.

Huang, J., Sun, M., Gumpper, K., Chi, Y., Ma, J., 2015. 3D multifocus astigmatism and compressed sensing (3D MACS) based superresolution reconstruction. Biomed. Opt Express 6 (3), 902. https://doi.org/10.1364/BOE.6.000902.

Huisken, J., Aug. 2004. Optical sectioning deep inside live embryos by selective plane illumination microscopy. Science (80- 305 (5686), 1007–1009. https://doi.org/10.1126/science.1100035.

Huynh, N., Zhang, E., Betcke, M., Arridge, S., Beard, P., Cox, B., 2016. Single-pixel optical camera for video rate ultrasonic imaging. Optica 3 (1), 26. https://doi.org/10.1364/optica.3.000026.

Ishigaki, K., Shiraishi, M., Suzuki, S., Asada, M., Nishiyama, N., Arai, S., 2012. Direct intensity modulation and wireless data transmission characteristics of terahertz-oscillating resonant tunnelling diodes. Electron. Lett. https://doi.org/10.1049/el.2012.0849.

Jacques, S.L., Jun. 2013. Optical properties of biological tissues: a review. Phys. Med. Biol. 58 (11), R37–R61. https://doi.org/10.1088/0031-9155/58/11/R37.

Jepsen, P.U., Cooke, D.G., Koch, M., 2011. Terahertz spectroscopy and imaging - modern techniques and applications. Laser Photon. Rev. 5 (1), 124–166. https://doi.org/10.1002/lpor.201000011.

Jin, A., Yazici, B., Ale, A., Ntziachristos, V., 2012. Preconditioning of the fluorescence diffuse optical tomography sensing matrix based on compressive sensing. Opt. Lett. 37 (20), 4326. https://doi.org/10.1364/ol.37.004326.

Jin, A., Yazici, B., Ntziachristos, V., 2014. Light illumination and detection patterns for fluorescence diffuse optical tomography based on compressive sensing. IEEE Trans. Image Process. 23 (6), 2609–2624. https://doi.org/10.1109/TIP.2014.2300756.

Jin, S., et al., Jun. 2016. Extended-field coverage hyperspectral camera based on a single-pixel technique. Appl. Opt. 55 (18), 4808. https://doi.org/10.1364/ao.55.004808.

Kelly, K., Takhar, T., DharmpalSun, Laska, J., Duarte, M., Baraniuk, R., 2007. "Abstract: D19.00007 : Compressed Sensing for Multispectral and Confocal Microscopy. BAPS.2007.MAR.D19.7.

Krishnan, D., Tay, T., Fergus, R., Jun. 2011. Blind deconvolution using a normalized sparsity measure. In: CVPR 2011, pp. 233–240. https://doi.org/10.1109/CVPR.2011.5995521.

Kuo, G., Linda Liu, F., Grossrubatscher, I., Ng, R., Waller, L., Mar. 2020. On-chip fluorescence microscopy with a random microlens diffuser. Opt Express 28 (6), 8384. https://doi.org/10.1364/OE.382055.

Li, X., Dyck, O., Kalinin, S.V., Jesse, S., Dec. 2018. Compressed sensing of scanning transmission electron microscopy (STEM) with nonrectangular scans. Microsc. Microanal. 24 (6), 623–633. https://doi.org/10.1017/S143192761801543X.

Li, W., et al., Dec. 2019. Single-frame wide-field nanoscopy based on ghost imaging via sparsity constraints. Optica 6 (12), 1515. https://doi.org/10.1364/OPTICA.6.001515.

Liu, Y., Suo, J., Zhang, Y., Dai, Q., 2018. Single-pixel phase and fluorescence microscope. Opt Express 26 (25), 32451. https://doi.org/10.1364/oe.26.032451.

Liu, X., et al., Sep. 2019. Fast fluorescence lifetime imaging techniques: a review on challenge and development. J. Innov. Opt. Health Sci. 12, 1930003. https://doi.org/10.1142/S1793545819300039, 05.

Lustig, M., Donoho, D.L., Santos, J.M., Pauly, J.M., Mar. 2008. Compressed sensing MRI. IEEE Signal Process. Mag. 25 (2), 72–82. https://doi.org/10.1109/MSP.2007.914728.

Ma, Y., Lee, Y., Best-Popescu, C., Gao, L., Jan. 2020. High-speed Compressed-Sensing Fluorescence Lifetime Imaging Microscopy of Live Cells. *bioRxiv*. https://doi.org/10.1101/2020.07.16.205161, 2020.07.16.205161.

Marcu, L., Feb. 2012. Fluorescence lifetime techniques in medical applications. Ann. Biomed. Eng. 40 (2), 304–331. https://doi.org/10.1007/s10439-011-0495-y.

Meiniel, W., et al., 2017. Reducing data acquisition for fast structured illumination microscopy using compressed sensing. In: Proceedings - International Symposium on Biomedical Imaging, pp. 32–35. https://doi.org/10.1109/ISBI.2017.7950461.

Mertz, J., 2011. Optical sectioning microscopy with planar or structured illumination. Nat. Methods 8 (10), 811–819. https://doi.org/10.1038/nmeth.1709.

Mizuno, T., Iwata, T., Apr. 2016. Hadamard-transform fluorescence-lifetime imaging. Opt Express 24 (8), 8202. https://doi.org/10.1364/OE.24.008202.

Moshtaghpour, A., Jacques, L., Cambareri, V., Antoine, P., Roblin, M., 2019. A variable density sampling scheme for compressive fourier transform interferometry. SIAM J. Imag. Sci. 12 (2), 671–715. https://doi.org/10.1137/18M1214111.

Nanni, E.A., et al., Dec. 2015. Terahertz-driven linear electron acceleration. Nat. Commun. 6 (1), 8486. https://doi.org/10.1038/ncomms9486.

Neifeld, M.A., Ke, J., Aug. 2007. Optical architectures for compressive imaging. Appl. Opt. 46 (22), 5293–5303. https://doi.org/10.1364/AO.46.005293.

Ntziachristos, V., Aug. 2006. Fluorescence molecular imaging. Annu. Rev. Biomed. Eng. 8 (1), 1–33. https://doi.org/10.1146/annurev.bioeng.8.061505.095831.

Ochoa, M., Pian, Q., Yao, R., Ducros, N., Intes, X., 2018. Assessing patterns for compressive fluorescence lifetime imaging. Opt. Lett. 43 (18), 4370. https://doi.org/10.1364/ol.43.004370.

Okhrimenko, M., Coburn, C., Hopkinson, C., Jun. 2019. Multi-spectral lidar: radiometric calibration, canopy spectral reflectance, and vegetation vertical SVI profiles. Rem. Sens. 11 (13), 1556. https://doi.org/10.3390/rs11131556.

Olarte, O.E., Andilla, J., Gualda, E.J., Loza-Alvarez, P., 2018. Light-sheet microscopy: a tutorial. Adv. Opt Photon 10 (1), 111. https://doi.org/10.1364/AOP.10.000111.

Oron, D., Tal, E., Silberberg, Y., 2005. Scanningless depth-resolved microscopy. Opt Express 13 (5), 1468. https://doi.org/10.1364/opex.13.001468.

Papagiakoumou, E., et al., 2013. Functional patterned multiphoton excitation deep inside scattering tissue. Nat. Photonics 7 (4), 274–278. https://doi.org/10.1038/nphoton.2013.9.

Parot, V.J., et al., Apr. 2019. Compressed Hadamard microscopy for high-speed optically sectioned neuronal activity recordings. J. Phys. D Appl. Phys. 52 (14), 144001. https://doi.org/10.1088/1361-6463/aafe88.

Pascucci, M., Ganesan, S., Tripathi, A., Katz, O., Emiliani, V., Guillon, M., Dec. 2019. Compressive three-dimensional super-resolution microscopy with speckle-saturated fluorescence excitation. Nat. Commun. 10 (1), 1327. https://doi.org/10.1038/s41467-019-09297-5.

Pavillon, N., Smith, N.I., 2016. Compressed sensing laser scanning microscopy. Opt Express 24 (26), 30038. https://doi.org/10.1364/oe.24.030038.

Pégard, N.C., Liu, H.-Y., Antipa, N., Gerlock, M., Adesnik, H., Waller, L., May 2016. Compressive light-field microscopy for 3D neural activity recording. Optica 3 (5), 517. https://doi.org/10.1364/optica.3.000517.

Pian, Q., Yao, R., Sinsuebphon, N., Intes, X., Jul. 2017. Compressive hyperspectral time-resolved wide-field fluorescence lifetime imaging. Nat. Photonics 11 (7), 411–414. https://doi.org/10.1038/nphoton.2017.82.

Radwell, N., Mitchell, K.J., Gibson, G.M., Edgar, M.P., Bowman, R., Padgett, M.J., 2014. Single-pixel infrared and visible microscope. Optica 1 (5), 285. https://doi.org/10.1364/optica.1.000285.

Ripoll, J., 2010. Hybrid Fourier-real space method for diffuse optical tomography. Opt. Lett. 35 (5), 688. https://doi.org/10.1364/ol.35.000688.

Rodríguez, A.D., Clemente, P., Irles, E., Tajahuerce, E., Lancis, J., 2014. Resolution analysis in computational imaging with patterned illumination and bucket detection. Opt. Lett. 39 (13), 3888. https://doi.org/10.1364/ol.39.003888.

Romberg, J., 2008. Imaging via compressive sampling: introduction to compressive sampling and recovery via convex programming. IEEE Signal Process. Mag. 25 (2), 14–20. https://doi.org/10.1109/MSP.2007.914729.

Rousset, F., Ducros, N., Farina, A., Valentini, G., D'Andrea, C., Peyrin, F., Mar. 2017. Adaptive basis scan by wavelet prediction for single-pixel imaging. IEEE Trans. Comput. Imaging 3 (1), 36–46. https://doi.org/10.1109/TCI.2016.2637079.

Rousset, F., Ducros, N., Peyrin, F., Valentini, G., D'Andrea, C., Farina, A., 2018. Time-resolved multispectral imaging based on an adaptive single-pixel camera. Opt Express 26 (8), 10550–10558 oe-26-8-10550.

Rowlands, C.J., et al., May 2017. Wide-field three-photon excitation in biological samples. Light Sci. Appl. 6 (5) https://doi.org/10.1038/lsa.2016.255 e16255–e16255.

Ruder, S., Sep. 2016. arXiv. An Overview of Gradient Descent Optimization Algorithms, vol. 1609, 04747.

Rudge, T.J., Soloviev, V.Y., Arridge, S.R., Mar. 2010. Fast image reconstruction in fluoresence optical tomography using data compression. Opt. Lett. 35 (5), 763. https://doi.org/10.1364/OL.35.000763.

Ruppert, D., Jun. 2004. The elements of statistical learning: data mining, inference, and prediction. J. Am. Stat. Assoc. 99 (466) https://doi.org/10.1198/jasa.2004.s339, 567–567.

Rust, M.J., Bates, M., Zhuang, X., 2006. Sub-diffraction-limit imaging by stochastic optical reconstruction microscopy (STORM). Nat. Methods 3 (10), 793–795. https://doi.org/10.1038/nmeth929.

Salvador-Balaguer, E., Latorre-Carmona, P., Chabert, C., Pla, F., Lancis, J., Tajahuerce, E., 2018. Low-cost single-pixel 3D imaging by using an LED array. Opt Express 26 (12), 15623. https://doi.org/10.1364/oe.26.015623.

Skodras, A., Christopoulos, C., Ebrahimi, T., 2001. The JPEG 2000 still image compression standard. IEEE Signal Process. Mag. 18 (5), 36–58. https://doi.org/10.1109/79.952804.

Soldevila, F., Clemente, P., Tajahuerce, E., Uribe-Patarroyo, N., Andrés, P., Lancis, J., Sep. 2016. Computational imaging with a balanced detector. Sci. Rep. 6 (1), 29181. https://doi.org/10.1038/srep29181.

Soldevila, F., et al., 2013. Single-pixel polarimetric imaging spectrometer by compressive sensing. Appl. Phys. B Laser Opt. 113 (4), 551–558. https://doi.org/10.1007/s00340-013-5506-2.

Soldevila, F., Salvador-Balaguer, E., Clemente, P., Tajahuerce, E., Lancis, J., 2015. High-resolution adaptive imaging with a single photodiode. Sci. Rep. 5 (1), 14300. https://doi.org/10.1038/srep14300.

Solomon, O., Mutzafi, M., Segev, M., Eldar, Y.C., 2018. Sparsity-based super-resolution microscopy from correlation information. Opt Express 26 (14), 18238. https://doi.org/10.1364/oe.26.018238.

Starck, J.-L., Bobin, J., Jun. 2010. Astronomical data analysis and sparsity: from wavelets to compressed sensing. Proc. IEEE 98 (6), 1021–1030. https://doi.org/10.1109/JPROC.2009.2025663.

Stevens, A., Yang, H., Carin, L., Arslan, I., Browning, N.D., Feb. 2014. The potential for bayesian compressive sensing to significantly reduce electron dose in high-resolution STEM images. Microscopy 63 (1), 41–51. https://doi.org/10.1093/jmicro/dft042.

Studer, V., Bobin, J., Chahid, M., Mousavi, H.S., Candes, E., Dahan, M., Jun. 2012. Compressive fluorescence microscopy for biological and hyperspectral imaging. Proc. Natl. Acad. Sci. Unit. States Am. 109 (26), E1679–E1687. https://doi.org/10.1073/pnas.1119511109.

Sun, M.-J., Zhang, J.-M., Feb. 2019. Single-pixel imaging and its application in three-dimensional reconstruction: a brief review. Sensors 19 (3), 732. https://doi.org/10.3390/s19030732.

Sun, B., Welsh, S.S., Edgar, M.P., Shapiro, J.H., Padgett, M.J., 2012. Normalized ghost imaging. Opt Express 20 (15), 16892. https://doi.org/10.1364/oe.20.016892.

Sun, M.J., Meng, L.T., Edgar, M.P., Padgett, M.J., Radwell, N., Dec. 2017. A Russian Dolls ordering of the Hadamard basis for compressive single-pixel imaging. Sci. Rep. 7 (1), 3464. https://doi.org/10.1038/s41598-017-03725-6.

Sun, T., et al., 2008. "Abstract: U36.00008 : Realization of Confocal and Hyper-spectral Microscopy via Compressive Sensing.

Sun, B., et al., May 2013. 3D computational imaging with single-pixel detectors. Science (80-.) 340 (6134), 844–847. https://doi.org/10.1126/science.1234454.

Tajahuerce, E., et al., 2014. Image transmission through dynamic scattering media by single-pixel photodetection. Opt Express 22 (14), 16945–16955. https://doi.org/10.1364/OE.22.016945.

Thompson, J.V., Mason, J.D., Beier, H.T., Bixler, J.N., Feb. 2017. "High speed fluorescence imaging with compressed ultrafast photography," in *high-speed biomedical Imaging and spectroscopy: toward big data Instrumentation and management II*, 10076, 1007613. https://doi.org/10.1117/12.2251025.

Van Ewout Berg, D.E.N., Friedlander, M.P., 2008. Probing the pareto frontier for basis pursuit solutions. SIAM J. Sci. Comput. 31 (2), 890–912. https://doi.org/10.1137/080714488.

Wadduwage, D.N., et al., May 2017. Near-common-path interferometer for imaging Fourier-transform spectroscopy in wide-field microscopy. Optica 4 (5), 546. https://doi.org/10.1364/optica.4.000546.

Waldchen, S., Lehmann, J., Klein, T., Van De Linde, S., Sauer, M., Dec. 2015. Light-induced cell damage in live-cell super-resolution microscopy. Sci. Rep. 5 (1), 15348. https://doi.org/10.1038/srep15348.

Wang, Y., Yang, B., Feng, S., Pessino, V., Huang, B., 2019. Multicolor fluorescent imaging by space-constrained computational spectral imaging. Opt Express 27 (4), 5393. https://doi.org/10.1364/oe.27.005393.

Wang, P., Liang, J., Wang, L.V., Dec. 2020. Single-shot ultrafast imaging attaining 70 trillion frames per second. Nat. Commun. 11 (1), 2091. https://doi.org/10.1038/s41467-020-15745-4.

Wang, C., et al., Oct. 2017. Computational spectral imaging based on compressive sensing. Chin. Phys. Lett. 34 (10), 104203. https://doi.org/10.1088/0256-307X/34/10/104203.

Watts, C.M., et al., 2014. Terahertz compressive imaging with metamaterial spatial light modulators. Nat. Photonics 8 (8), 605–609. https://doi.org/10.1038/nphoton.2014.139.

Weissleder, R., Ntziachristos, V., 2003. Shedding light onto live molecular targets. Nat. Med. 9 (1), 123–128. https://doi.org/10.1038/nm0103-123.

Wen, C., Ren, M., Feng, F., Chen, W., Chen, S.-C., 2019. Compressive sensing for fast 3-D and random-access two-photon microscopy. Opt. Lett. 44 (17), 4343. https://doi.org/10.1364/ol.44.004343.

Wijesinghe, P., Escobet-Montalbán, A., Chen, M., Munro, P.R.T., Dholakia, K., Oct. 2019. Optimal compressive multiphoton imaging at depth using single-pixel detection. Opt. Lett. 44 (20), 4981–4984. https://doi.org/10.1364/OL.44.004981.

Wilcox, D.S., Buzzard, G.T., Lucier, B.J., Rehrauer, O.G., Wang, P., Ben-Amotz, D., 2013. Digital compressive chemical quantitation and hyperspectral imaging. Analyst 138 (17), 4982. https://doi.org/10.1039/c3an00309d.

Woringer, M., Darzacq, X., Zimmer, C., Mir, M., 2017. Faster and less phototoxic 3D

fluorescence microscopy using a versatile compressed sensing scheme. Opt Express 25 (12), 13668. https://doi.org/10.1364/oe.25.013668.

Wu, Y., Ye, P., Mirza, I.O., Arce, G.R., Prather, D.W., 2010. Experimental demonstration of an optical-sectioning compressive sensing microscope (CSM). Opt Express 18 (24), 24565. https://doi.org/10.1364/oe.18.024565.

Wu, J., Li, S., Zhang, S., Lin, D., Yu, B., Qu, J., 2018. Fast analysis method for stochastic optical reconstruction microscopy using multiple measurement vector model sparse Bayesian learning. Opt. Lett. 43 (16), 3977. https://doi.org/10.1364/ol.43.003977.

Xu, Y., Chen, J., Liyang, L., Kelly, K.F., Aug. 2018. Compressive hyperspectral microscopy of nanomaterials. In: 2018 IEEE Research and Applications of Photonics in Defense Conference (RAPID), pp. 1–3. https://doi.org/10.1109/RAPID.2018.8509015.

Yang, S., Lee, J., Lee, Y., Lee, M., Lee, B.-U., 2015a. Estimation of multiexponential fluorescence decay parameters using compressive sensing. J. Biomed. Opt. 20 (9), 096003 https://doi.org/10.1117/1.jbo.20.9.096003.

Yang, F., Zhao, L., Cong, W., Wang, G., Intes, X., 2015b. High-resolution mesoscopic fluorescence molecular tomography based on compressive sensing. IEEE Trans. Biomed. Eng. 62 (1), 248–255. https://doi.org/10.1109/TBME.2014.2347284.

Yang, F., Yao, R., Ozturk, M.S., Faulkner, D., Qu, Q., Intes, X., Jun. 2018. Improving mesoscopic fluorescence molecular tomography via preconditioning and regularization. Biomed. Opt Express 9 (6), 2765. https://doi.org/10.1364/BOE.9.002765.

Yanny, K., et al., Dec. 2020. Miniscope3D: optimized single-shot miniature 3D fluorescence microscopy. Light Sci. Appl. 9 (1), 171. https://doi.org/10.1038/s41377-020-00403-7.

Yao, R., Pian, Q., Intes, X., Dec. 2015. Wide-field fluorescence molecular tomography with compressive sensing based preconditioning. Biomed. Opt Express 6 (12), 4887. https://doi.org/10.1364/BOE.6.004887.

Yao, R., Intes, X., Fang, Q., Jan. 2016. Generalized mesh-based Monte Carlo for wide-field illumination and detection via mesh retessellation. Biomed. Opt Express 7 (1), 171. https://doi.org/10.1364/BOE.7.000171.

Yao, R., Ochoa, M., Yan, P., Intes, X., "Net-Flics, Dec. 2019. Fast quantitative wide-field fluorescence lifetime imaging with compressed sensing − a deep learning approach. Light Sci. Appl. 8 (1), 26. https://doi.org/10.1038/s41377-019-0138-x.

Ye, P., Paredes, J.L., Arce, G.R., Wu, Y., Chen, C., Prather, D.W., Apr. 2009. Compressive confocal microscopy. In: 2009 IEEE International Conference on Acoustics, Speech and Signal Processing, pp. 429–432. https://doi.org/10.1109/ICASSP.2009.4959612.

Yuan, X., Pang, S., 2016. Structured illumination temporal compressive microscopy. Biomed. Opt Express 7 (3), 746. https://doi.org/10.1364/BOE.7.000746.

Zhang, Z., Ma, X., Zhong, J., May 2015. Single-pixel imaging by means of Fourier spectrum acquisition. Nat. Commun. 6 (1), 6225. https://doi.org/10.1038/ncomms7225.

Zhang, Z., Wang, X., Zheng, G., Zhong, J., Aug. 2017. Hadamard single-pixel imaging versus Fourier single-pixel imaging. Opt Express 25 (16), 19619. https://doi.org/10.1364/OE.25.019619.

Zhang, S., Wu, J., Chen, D., Li, S., Yu, B., Qu, J., Feb. 2019. Fast frequency-domain compressed sensing analysis for high-density super-resolution imaging using orthogonal matching pursuit. IEEE Photonics J. 11 (1), 1–8. https://doi.org/10.1109/JPHOT.2018.2884730.

Zhao, L., Yang, H., Cong, W., Wang, G., Intes, X., 2014. L_p regularization for early gate fluorescence molecular tomography. Opt. Lett. 39 (14), 4156. https://doi.org/10.1364/ol.39.004156.

Zhu, D., Li, C., 2014. Nonconvex regularizations in fluorescence molecular tomography for sparsity enhancement. Phys. Med. Biol. 59 (12), 2901–2912. https://doi.org/10.1088/0031-9155/59/12/2901.

Zhu, G., van Howe, J., Durst, M., Zipfel, W., Xu, C., 2005. Simultaneous spatial and temporal focusing of femtosecond pulses. In: Conference on Lasers and Electro-Optics/Quantum Electronics and Laser Science and Photonic Applications Systems Technologies, p. CWP1.

Zhu, L., Zhang, W., Elnatan, D., Huang, B., Jul. 2012. Faster STORM using compressed sensing. Nat. Methods 9 (7), 721–723. https://doi.org/10.1038/nmeth.1978.

Zimmermann, T., Rietdorf, J., Pepperkok, R., Jul. 2003. Spectral imaging and its applications in live cell microscopy. FEBS Lett. 546 (1), 87–92. https://doi.org/10.1016/S0014-5793(03)00521-0.